European Journal of Pharmaceutics and Biopharmaceutics 142 (2019) 70–82

Contents lists available at ScienceDirect

European Journal of Pharmaceutics and Biopharmaceutics

journal homepage: www.elsevier.com/locate/ejpb

Research paper

Protein-functionalized nanoparticles derived from end-functional polymers and polymer prodrugs for crossing the blood-brain barrier

Alysia Cox[a,1], Daniele Vinciguerra[b,1], Francesca Re[a,*], Roberta Dal Magro[a], Simona Mura[b], Massimo Masserini[a], Patrick Couvreur[b], Julien Nicolas[b,*]

[a] School of Medicine and Surgery, Nanomedicine Center NANOMIB, University of Milano-Bicocca, Via Raoul Follereau 3, 20854 Vedano al Lambro, MB, Italy
[b] Institut Galien Paris-Sud, UMR CNRS 8612, Univ Paris-Sud, Faculté de Pharmacie, 5 rue Jean-Baptiste Clément, F-92296 Châtenay-Malabry cedex, France

ARTICLE INFO

Keywords:
Polymer
Prodrug
Nanoparticle
Blood-brain barrier
Proteins
Drug delivery

ABSTRACT

Nanoparticles may provide a viable way for neuroprotective drugs to cross the blood–brain barrier (BBB), which limits the passage of most drugs from the peripheral circulation to the brain. Heterotelechelic polymer prodrugs comprising a neuroprotective model drug (adenosine) and a maleimide functionality were synthesized by the "*drug-initiated*" approach and subsequent nitroxide exchange reaction. Nanoparticles were obtained by nanoprecipitation and exhibited high colloidal stability with diameters in the 162–185 nm range and narrow size distributions. Nanoparticles were then covalently surface-conjugated to different proteins (albumin, α2-macroglobulin and fetuin A) to test their capability of enhancing BBB translocation. Their performances in terms of endothelial permeability and cellular uptake in an *in vitro* BBB model were compared to that of similar nanoparticles with surface-adsorbed proteins, functionalized or not with the drug. It was shown that bare NPs (i.e., NPs not surface-functionalized with proteins) without the drug exhibited significant permeability and cellular uptake, which were further enhanced by NP surface functionalization with α2-macroglobulin. However, the presence of the drug at the polymer chain-end prevented efficient passage of all types of NPs through the BBB model, likely due to a decrease in the hydrophobicity of the nanoparticle surface and alteration of the protein binding/coupling, respectively. These results established a new and facile synthetic approach for the surface-functionalization of polymer nanoparticles for brain delivery purposes.

1. Introduction

The blood–brain barrier (BBB) remains one of the major limiting obstacles preventing pharmacological advancement in the treatment of neurological, neurodegenerative, and psychiatric disorders [1]. Although nanoparticles (NP) offer a promising approach to cross this barrier, surface-modification is necessary to increase drug delivery to the central nervous system (CNS). With this in mind, synthetic and physiological peptides and proteins have extensively been used to coat or functionalize NPs for BBB targeting [2–4]. Many techniques have been utilized to identify novel synthetic peptides or previously untested physiological proteins, including peptide phage display and computer-assisted design [5]. A wide array of these ligands has been successfully used to target receptor-mediated endocytosis and encourage passage of NPs through the BBB [6], commonly through transferrin receptor [7–9], lactoferrin receptor [10,11], and low-density lipoprotein receptor (LDLr) [12,13]. In particular, a modified fragment of apolipoprotein E, named mApoE, successfully enhanced brain delivery of liposomes designed for the treatment of Alzheimer's disease *via* transcytosis targeting LDLr [12,13].

We recently analyzed the protein composition of NP corona after passage through an *in vitro* BBB model and found that specific proteins were able to cross endothelial BBB cells in relatively high abundance [14]. Among these proteins, we have selected three to test their capability to improve brain targeting of polymeric NP: albumin, α_2-macroglobulin (α2M) and Fetuin A (Fet A). Albumin, the most abundant serum protein, crosses the BBB *in vivo* in healthy conditions [15], and in higher quantities after traumatic brain injury [16], in Huntington disease [17], diabetes and dementia [18]. α2M is a broad spectrum antiprotease that also crosses the healthy BBB [19] and is a biomarker for multiple sclerosis [20]. It has anti-inflammatory effects which seem particularly promising in treating neurological conditions that are coupled with increased local or generalized inflammation [21]. Fet A, also known as α_2-HS-glycoprotein, is predominantly found in fetal

* Corresponding authors.
E-mail addresses: francesca.re1@unimib.it (F. Re), julien.nicolas@u-psud.fr (J. Nicolas).
[1] Equally contributing authors.

https://doi.org/10.1016/j.ejpb.2019.06.004
Received 18 March 2019; Received in revised form 30 May 2019; Accepted 6 June 2019
Available online 06 June 2019

serum where it prevents tissue calcification [22]. It can cross the BBB during ischemic injury [23]. Although albumin has previously been used to synthesize NPs that can cross the BBB [24], the use of α2M or Fet A for functionalizing NPs to specifically target the brain has never been investigated.

Among the different families of materials suitable for the design of targeted drug delivery systems, polymer NPs have attracted much attention because of their numerous benefits. Polymer synthesis methods indeed offer great flexibility in terms of control, macromolecular architecture, physico-chemical properties, and enable easy access to functional materials. For instance, different polymer NPs have been engineered to allow surface modification for CNS drug delivery with various ligands to enhance their permeability through the BBB [25–27]. NP coating by simple adsorption of targeting peptides has been extensively investigated [28–30], but surface functionalization *via* covalent linkage remains the method of choice as it prevents protein desorption and loss of targeting, though it requires more elaborate synthetic strategies. Developing polymer prodrug nanocarriers, where the drug is linked to the polymer, usually comes with important benefits compared to traditional drug-loaded systems [31], including: (i) absence of "burst release" (i.e., uncontrolled release of drugs post-administration); (ii) the possibility to obtain higher drug loading and (iii) enhancement of the drug compatibility with the polymer matrix/core, allowing a broader range of drugs to be transported.

Heterotelechelic polymers are gaining great interest in the biomedical field [32], as they offer an opportunity to embed two different biologically active moieties positioned at both extremities (e.g., drug, targeting ligands, imaging probes). In this context, we proposed the synthesis of heterotelechelic polymers bearing a drug of interest in the β-position and a reactive group for further conjugation with BBB-crossing proteins in the ω-position.

As a proof of concept, adenosine (Ade) was chosen as a model drug for this drug delivery system. Its neuroprotective characteristics have already been demonstrated *in vivo* after stroke when delivered to BBB endothelial cells as a squalene-Ade molecular prodrug [33].

Here, we either adsorb or conjugate bovine serum albumin (BSA), α2M or Fet A at the surface of heterobifunctional polymer prodrug NPs (Fig. 1) and report on the proteins effect on NP ability to cross the *in vitro* BBB, possibly enhancing Ade transport and therefore its neuroprotective activity. Moreover, targeting is vital to avoid side reactions, given the widespread expression of Ade receptors throughout the body [34,35], and peripheral degradation [36]. Though investigation of the pharmacological activity of the prodrug NPs is outside the scope of this article, we investigate here the possibility to embed a relevant drug for the treatment of CNS-related diseases and study its impact on the nanoparticle interaction/functionalization with proteins, and their subsequent cellular uptake and permeability through a well-established and widely used *in vitro* transwell BBB model [3].

2. Materials and methods

2.1. Materials

Adenosine, *tert*-Butyldimethylsilyl chloride (TBDMSCl), imidazole, *N,N*-diisopropylethylamine (DIPEA), isoprene, 4-(dimethylamino)pyridine (DMAP), succinic anhydride, 4-hydroxy-TEMPO, 1-[bis(dimethylamino)methylene]-1H-1,2,3-triazolo[4,5-b]pyridinium 3-oxid hexafluorophosphate (HATU), rhodamine B base (Rho), *N*-(3-Dimethylaminopropyl)-*N'*-ethylcarbodiimide hydrochloride (EDC·HCl), *exo*-3,6-epoxy-1,2,3,6-tetrahydrophthalic anhydride, 2-(2-aminoethoxy)-ethanol as well as dry solvents, corning transwells (polystyrene membrane, 12 well plates, 0.4 μm pores), bovine α2M, bovine fetuin (Fet A), bovine serum albumin (BSA) and cell medium components were purchased from Sigma-Aldrich (Lyon, France) and used as received. Tetrabutylammonium fluoride (TBAF) was purchased from Alfa Aesar (Kandel, Germany). *N-tert*-butyl-*N*-(1-diethylphosphono-2,2-dimethylpropyl) nitroxide (SG1, 85%) was kindly supplied by Arkema. AMA-SG1 alkoxyamine [37], Rho-TEMPO [38] and tris-O-silylated adenosine [39] were prepared as reported previously. All other reactants were purchased from Sigma-Aldrich (Lyon, France) at the

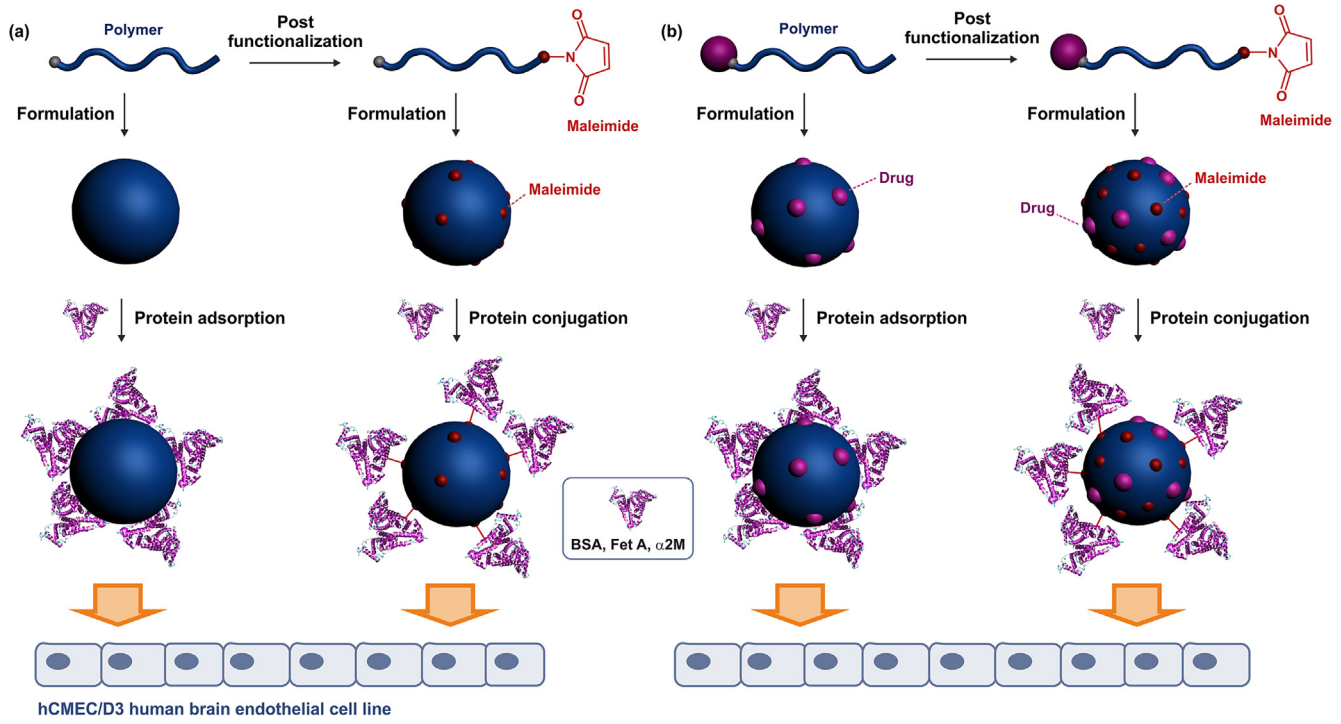

Fig. 1. General strategies for the preparation of (a) polymer nanoparticles and (b) polymer prodrug nanoparticles surface-adsorbed or surface-functionalized with proteins for the crossing of hCMEC/D3 human brain endothelial cells as a blood–brain barrier (BBB) model. BSA = albumin, α2M = α2-macroglobulin and Fet A = fetuin A.

highest available purity and used as received. Deuterated chloroform ($CDCl_3$) was obtained from Eurisotop (France). All other solvents were purchased from Carlo-Erba (France) at the highest grade. EBM-2 basal medium was from Lonza (Switzerland). Nanosep centrifugal devices (Omega membrane, 300 K) were from VWR International (Fontenay-sous-Bois, France). BCA assay kit was from Thermo Fisher Scientific (Illkirch, France). hCMEC/D3 cells were provided by Pierre-Olivier Couraud (Université Paris Descartes, Paris, France). FITC-dextran 40 kDa was purchased from Sigma-Aldrich (Milan, Italy).

2.2. Analytical methods

Nuclear Magnetic Resonance Spectroscopy (NMR). NMR spectroscopy was performed in 5 mm diameter tubes in $CDCl_3$ at 25 °C. ^1H and ^{13}C NMR spectroscopy was performed on a Bruker Avance 300 spectrometer at 300 MHz (^1H) or 75 MHz (^{13}C). The chemical shift scale was calibrated based on the internal solvent signals. To characterize nitroxide derivatives, pentafluorophenylhydrazine was added *in situ* and allowed to react before the analysis [40,41].

Mass spectrometry. Mass spectra were recorded with a Bruker Esquire-LC instrument. High-resolution mass spectra (ESI) were recorded on an ESI/TOF (LCT, Waters) LC-spectrometer.

Size Exclusion Chromatography (SEC). SEC was performed at 30 °C with two columns from Polymer Laboratories (PL-gel MIXED-D; 300 × 7.5 mm; bead diameter 5 mm; linear part 400 to 4×10^5 g mol^{-1}), a differential refractive index detector (Spectra System RI-150 from Thermo Electron Corp.) and a scanning fluorescence detector (Waters 474). The eluent was chloroform at a flow rate of 1 mL min^{-1} (Waters 515 pump) and toluene was used as a flow-rate marker. The calibration curve was based on polystyrene (PS) standards (peak molar masses, M_p = 162–523 000 g mol^{-1}) from Polymer Laboratories. A *polyisoprene* (PI) calibration curve was constructed by converting the PS standard peak molecular weights (M_{PS}) to PI molecular weights (M_{PI}) using Mark-Houwink-Sakurada (MHS) constants determined for both polymers in CCl_4 at 25 °C. For PI, the MHS constants used were $K_{PI} = 2.44 \times 10^4$ and $\alpha_{PI} = 0.712$. For PS, $K_{PS} = 7.1 \times 10^4$ and $\alpha_{PS} = 0.54$ ($M_w < 16\ 700$ g.mol^{-1}) or $K_{PS} = 1.44 \times 10^4$ and $\alpha_{PS} = 0.713$ ($M_w > 16\ 700$ g mol^{-1}) [42]. This technique allowed the number-average molar mass (M_n), the weight-average molar mass (M_w) and the dispersity (M_w/M_n, $Đ$) to be determined.

Dynamic Light Scattering (DLS) and zeta potential. Nanoparticle diameters (*Dz*) and zeta potentials (ζ) were measured by dynamic light scattering (DLS) with a Nano ZS from Malvern (173° scattering angle) at a temperature of 25 °C. The surface charge of the NPs was investigated by ζ-potential (mV) measurement at 25 °C after dilution with 1 mM NaCl, using the Smoluchowski equation.

2.3. Synthesis

Synthesis of PI. AMA-SG1 (120 mg, 0.327 mmol) was placed in a 15 mL-capacity pressure tube (Ace Glass 8648–164) fitted with a plunger valve and thermowell. After addition of isoprene (6.5 mL, 6.53 mmol) and dry 1,4-dioxane (6.5 mL), the tube underwent three cycles of freeze-thaw degassing and was then backfilled with argon. The tube was placed in a preheated oil bath at 115 °C for 16 h (**PI1**) and then cooled to r.t. by placing it under cold water. The residue was concentrated under reduced pressure and precipitated in cold methanol to give PI as a colorless viscous oil. Two other polymerizations were performed for 16 h with $[isoprene]_0/[AMA\text{-}SG1]_0$ = 500/1 (**PI2**) and 400/1 (**PI3**). All polymers were characterized by SEC and ^1H NMR. **PI1**: $M_{n,SEC}$ = 2860 g mol^{-1}, $Đ$ = 1.13. **PI2**: $M_{n,SEC}$ = 4940 g mol^{-1}, $Đ$ = 1.18. **PI3**: $M_{n,SEC}$ = 4320 g mol^{-1}, $Đ$ = 1.16.

Synthesis of PI-Rho. Briefly, **PI1** (300 mg, 0.105 mmol, 1 eq) and TEMPO-Rho (72 mg, 0.105 mmol, 1 eq) were placed in a 7 mL-vial and dissolved in dry pyridine (1 mL). After 20 min of degassing under argon, the vial was placed in a preheated oil bath at 110 °C and stirred for 16 h. **PI-Rho** was then precipitated two times in cold methanol and dried under reduced pressure until constant weight. Functionalization was confirmed by SEC equipped with a fluorescent detector (λ_{ex} = 570 nm, λ_{em} = 595 nm). $M_{n,SEC}$ = 2690 g mol^{-1}, $Đ$ = 1.13.

Synthesis of PI-OH. Briefly, **P2** (0.500 g, 0.101 mmol, 1 eq) and 4-hydroxy-TEMPO (0.017 g, 0.101 mmol, 1 eq) were placed in a 7 mL-vial and dissolved in 1 mL of dry pyridine. After 20 min of degassing under argon, the vial was placed in a preheated oil bath at 110 °C and stirred for 16 h. **PI-OH** was then precipitated two times in cold methanol and dried under reduced pressure until constant weight. The polymer was characterized by SEC and ^1H NMR. $M_{n,SEC}$ = 5030 g mol^{-1}, $Đ$ = 1.15.

Synthesis of *N*-[2-(2-hydroxyethoxy)ethyl]-*exo*-3,6-epoxy-1,2,3,6-tetrahydrophthalimide. *N*-[2-(2-Hydroxyethoxy)ethyl]-*exo*-3,6-epoxy-1,2,3,6-tetrahydrophthalimide was prepared according to a modified published procedure [43]. *Exo*-3,6-epoxy-1,2,3,6-tetrahydrophthalic anhydride (0.50 g, 3.01 mmol) was dissolved in 2-(2-aminoethoxy)-ethanol (1.58 g, 15.0 mmol) and stirred at 80 °C for 7 h. The reaction mixture was cooled to r.t. before addition of DCM. The solution was washed with brine, dried over $MgSO_4$ and concentrated to give a colorless oil. Yield: 39% (0.318 g.). ^1H NMR (300 MHz, $CDCl_3$) δ 6.51 (s, 2H), 5.29 (s, 2H), 3.76–3.50 (m, 8H), 2.87 (s, 2H), 2.59 (b, 1H) ppm. ^{13}C NMR (75 MHz, $CDCl_3$) δ 176.38, 136.30, 81.02, 72.25, 67.06, 61.63, 47.40, 38.58.

Synthesis of succinic-mal-furan (*N*-[2-(2-hydroxyethoxy) ethyl]-*exo*-3,6-epoxy-1,2,3,6-tetrahydrophthalimide-4-oxobutanoic acid). Succinic-mal-furan was prepared according to a modified published procedure [44]. Briefly, a solution of DMAP (0.290 g, 2.37 mmol) and succinic anhydride (0.237 g, 2.37 mmol) in dry DCM (10 mL) was added dropwise at 0 °C and under an argon atmosphere, to a solution of *N*-[2-(2-hydroxyethoxy)ethyl]-*exo*-3,6-epoxy-1,2,3,6-tetrahydrophthalimide (0.200 g, 0.833 mmol) in dry DCM (2 mL). After stirring overnight at r.t., the solution was quenched with 1 M HCl. The product was extracted three times with DCM. The combined organic layers were washed with brine and dried over $MgSO_4$. After evaporation of the solvent, succinic-mal-furan was obtained as a white solid. Yield: 96%. ^1H NMR ($CDCl_3$, 300 MHz): δ 6.53 (s, 2H), 5.30 (d, 2H), 4.27 – 4.15 (m, 2H), 3.66 (dq, 6H), 2.90 (s, 2H), 2.68 (s, 4H). ^{13}C NMR (75 MHz, $CDCl_3$) δ 176.39, 171.95, 136.54, 80.77, 68.50, 67.05, 63.81, 47.49, 38.24, 29.05, 28.88. MS (ESI-): m/z = 352.2 $(M)^-$. Calc. for $C_{16}H_{19}NO_8$: 353.1.

Synthesis of PI-mal-furan. A solution of succinic-mal-furan (0.043 g, 0,121 mmol, 2 eq), EDC·HCl (0.023 g, 0.121 mmol, 2 eq) and DMAP (cat) in dry DCM (1 mL) was stirred for 15 min and added dropwise to a solution of **PI-OH** (0. 300 g, 0.061 mmol, 1 eq) in DCM (1 mL). The mixture was stirred overnight under argon at r.t., before being quenched with water and extracted with DCM. The organic phases were then washed with brine and dried with $MgSO_4$. After evaporation of the solvent, two precipitation in cold methanol were performed to obtain PI-mal-furan as a colorless oil. The polymer was characterized by SEC and ^1H NMR. $M_{n,SEC}$ = 5200 g mol^{-1}, $Đ$ = 1.15.

Synthesis of PI-mal. PI-mal-furan (0.200 g, 0.038 mmol) was dissolved in dry toluene (1 mL). After 20 min of degassing under argon, the vial was placed in a preheated oil bath at 100 °C and stirred for 16 h. **PI-mal** was then precipitated two times in cold methanol and dried under reduced pressure until constant weight. The polymer was characterized by SEC and ^1H NMR, which also confirmed the disappearance of the maleimide protecting group. $M_{n,SEC}$ = 5650 g mol^{-1}, $Đ$ = 1.17.

Synthesis of tris-O-silylated adenosine-AMA-SG1 (TBDMS-Ade-AMA-SG1). Tris-O-silylated adenosine (TBDMS-Ade, 2.0 g, 3.28 mmol) was dissolved in 10 mL of dry DMF. HATU (2.49 g, 6.56 mmol) and AMA-SG1 (2.37 g, 6.56 mmol) were dissolved in 10 mL of dry DMF in another round-bottomed flask, DIPEA (2.12 g, 16.4 mmol) was added dropwise by syringe. The mixture was stirred for 1 h and added by syringe to the first solution. The solution was stirred under argon atmosphere for 96 h at room temperature (r.t.), then diluted with 100 mL

EtOAc. The organic phase was washed with 1 M HCl, sat. $NaHCO_3$ aqueous solution, and brine before being dried over $MgSO_4$. The residue was concentrated under reduced pressure and purified by flash chromatography (SiO_2, gradient from PetrolEther/EtOAc 9/1 v/v to PetrolEther/EtOAc 5/5 as eluent) to give 1.95 g of TBDMS-Ade-AMA-SG1 as a white-yellow solid. Yield: 62%. ^{1}H NMR ($CDCl_3$, 300 MHz): δ 11.01 (d, 1H), 8.76 (s, 1H), 8.31 (d, 1H), 6.09 (m, 1H), 4.93–4.82 (d, 1H), 4.69 (dt, 1H), 4.37–4.29 (m, 2H), 4.23–3.98 (m, 5H), 3.81 (dt, 1H), 3.49 (d, 1H), 1.62 (d, 3H), 1.32 (t, 6H), 1.22–1.20 (m, 18H), 0.95 (d, 18H), 0.81 (d, 9H), 0.12 (d, 12H), −0.03 (d, 3H), −0.24 (d, 3H) ppm. ^{13}C NMR (75 MHz, $CDCl_3$): δ 169.75, 152.42, 152.06, 149.66, 141.76, 88.39, 85.51, 85.19, 78.82, 78.69, 75.58, 72.02, 71.72, 70.04, 68.21, 62.63, 62.44, 61.82, 60.65, 35.41, 30.54, 28.24, 26.08, 25.85, 25.68, 18.50, 18.08, 17.83, 16.50, 16.23, −4.40, −4.71, −5.05, −5.39 ppm. MS (ESI +): m/z = 981.6 $(M + Na)^+$. Calc. for $C_{29}H_{48}N_3O_7P$: 958.6.

Synthesis of TBDMS-Ade-PI. TBDMS-Ade-AMA-SG1 (110 mg, 0.115 mmol) was placed in a 15 mL-capacity pressure tube (Ace Glass 8648–164) fitted with plunger valves and thermowells. After addition of isoprene (5.7 mL, 57.2 mmol) and dry 1,4-dioxane (5.7 mL), the tube underwent three cycles of freeze-thaw degassing and was then backfilled with argon. The tube was then placed in a preheated oil bath at 115 °C for 16 h (**TBDMS-Ade-PI1**) and cooled to r.t. by placing under cold water. The residue was concentrated under reduced pressure and precipitated in cold methanol to give TBDMS-Ade-PI as a colorless viscous oil. Another polymerization was performed for 16 h with $[isoprene]_0/[TBDMS\text{-}Ade\text{-}AMA\text{-}SG1]_0$ = 780/1 (**TBDMS-Ade-PI2**). All polymers were characterized by SEC and ^{1}H NMR. $M_{n,NMR}$ was calculated according to $M_{n,NMR} = (DP_{n,NMR} \times MW_{isoprene}) + MW_{TBDMS\text{-}Ade\text{-}AMA\text{-}SG1}$ with $DP_{n,NMR}$ calculated from the ratio of areas under the peak at 8.69, 8.31 and 5.98 ppm (aromatic and anomeric proton of Ade) and 5.0–5.5 ppm (vinylic H in isoprene repeat unit (1,4-addition), corresponding to ~ 81% of total isoprene units [37]). **TBDMS-Ade-PI1**: $M_{n,SEC}$ = 6000 g mol^{-1}, $M_{n,NMR}$ = 6450 g mol^{-1} and $Đ$ = 1.16. **TBDMS-Ade-PI2**: $M_{n,SEC}$ = 5100 g mol^{-1}, $M_{n,NMR}$ = 5050 g mol^{-1}, and $Đ$ = 1.16.

Synthesis of Ade-PI. The TBDMS-protected **TBDMS-Ade-PI2** (0.300 g, 0.050 mmol) was dissolved in 1.5 mL THF and TBAF (1 M in THF, 150 µL) was added. The solution was stirred for 30 min and then purified by two consecutive precipitation in cold methanol to give **Ade-PI** as a colorless viscous oil. The polymer was characterized by SEC and ^{1}H NMR, which confirmed also the disappearance of TBDMS protecting groups. $M_{n,NMR}$ was calculated according to $M_{n,NMR} = (DP_{n,NMR} \times MW_{isoprene}) + MW_{TBDMS\text{-}Ade\text{-}AMA\text{-}SG1} - MW_{TBDMS}$ with $DP_{n,NMR}$ calculated from ratio of areas under the peak at 8.69, 8.31 and 5.98 ppm (aromatic and anomeric proton of Ade) and 5.0–5.5 ppm (vinylic H in isoprene repeat unit (1,4-addition), corresponding to ~ 81% of total isoprene units [37]). $M_{n,SEC}$ = 6260 g mol^{-1}, $M_{n,NMR}$ = 6280 g mol^{-1}, $Đ$ = 1.15.

Synthesis of TBDMS-Ade-PI-OH. Briefly, **TBDMS-Ade-PI1** (0.500 g, 0.098 mmol, 1 eq) and 4-hydroxy-TEMPO (0.017 g, 0.098 mmol, 1 eq) were placed in a 7 mL-vial and dissolved in 1 mL of dry pyridine. After 20 min of degassing under argon, the vial was placed in a preheated oil bath at 110 °C and stirred for 16 h. **TBDMS-Ade-PI-OH** was then precipitated two times in cold methanol and dried under reduced pressure until constant weight. The polymer was characterized by SEC and ^{1}H NMR. $M_{n,NMR}$ was calculated according to $M_{n,NMR} = (DP_{n,NMR} \times MW_{isoprene}) + MW_{TBDMS\text{-}Ade\text{-}AMA\text{-}SG1} - MW_{SG1} + MW_{TEMPO\text{-}OH}$ with $DP_{n,NMR}$ calculated from ratio of areas under the peak at 8.69, 8.31 and 5.98 ppm (aromatic and anomeric proton of Ade) and 5.0–5.5 ppm (vinylic H in isoprene repeat unit (1,4-addition), corresponding to ~ 81% of total isoprene units [37]). $M_{n,SEC}$ = 5330 g mol^{-1}, $M_{n,NMR}$ = 7590 g mol^{-1}, $Đ$ = 1.15.

Synthesis of TBDMS-Ade-PI-mal-furan. A solution of succinic-mal-furan (0.041 g, 0.117 mmol, 2 eq), EDC·HCl (0.022 g, 0.117 mol, 2 eq) and DMAP (cat) in dry DCM (1 mL) was stirred for 15 min and added dropwise to a solution of **TBDMS-Ade-PI-OH** (0.300 g, 0.059 mmol, 1 eq) in dry DCM (1 mL). The mixture was stirred overnight under argon at r.t., before being quenched with water and extracted with DCM. The organic phases were then washed with brine and dried with $MgSO_4$. After evaporation of the solvent, two precipitations in cold methanol were performed to obtain TBDMS-Ade-PI-mal-furan as a colorless oil. The polymer was characterized by SEC and ^{1}H NMR. The post-functionalization yield was calculated by ^{1}H NMR using the chemical shifts of protons of mal (δ = 6.53, 4.22, 2.90 and 2.68 ppm) and the chemical shifts of aromatic protons and anomeric proton of Ade (δ = 8.69, 8.31 and 5.98 ppm). $M_{n,NMR}$ was calculated according to $M_{n,NMR} = (DP_{n,NMR} \times MW_{isoprene}) + MW_{TBDMS\text{-}Ade\text{-}AMA\text{-}SG1} - MW_{SG1} + MW_{TEMPO\text{-}mal\text{-}furan}$ with $DP_{n,NMR}$ calculated from ratio of areas under the peak at 8.69, 8.31 and 5.98 ppm (aromatic and anomeric proton of Ade) and 5.0–5.5 ppm (vinylic H in isoprene repeat unit (1,4-addition), corresponding to ~ 81% of total isoprene units [37]). $M_{n,SEC}$ = 5370 g mol^{-1}, $M_{n,NMR}$ = 9120 g mol^{-1}, $Đ$ = 1.15.

Synthesis of Ade-PI-mal-furan. The TBDMS-protected **TBDMS-Ade-PI-mal-furan** (0.300 g, 0.056 mmol) was dissolved in 1.5 mL THF and TBAF (1 M in THF, 150 µL) was added. The solution was stirred for 30 min and then purified by two consecutive precipitations in cold methanol to give Ade-PI-mal-furan as a colorless viscous oil. It was then directly used for the next reaction.

Synthesis of Ade-PI-mal. Ade-PI-mal-furan (0.200 g, 0.036 mmol) was dissolved in dry toluene (1 mL). After 20 min of degassing under argon, the vial was placed in a preheated oil bath at 100 °C and stirred for 16 h. **Ade-PI-mal** was then precipitated two times in cold methanol and dried under reduced pressure until constant weight. The polymer was characterized by SEC and ^{1}H NMR, which also confirmed the disappearance of maleimide protecting group. The post-functionalization yield was calculated by ^{1}H NMR from ratio of areas under the peak of protons of mal at 6.53, 4.22, 2.90 and 2.68 ppm and aromatic and anomeric protons of Ade at 8.69, 8.31 and 5.98 ppm. $M_{n,NMR}$ was calculated according to $M_{n,NMR} = (DP_{n,NMR} \times MW_{isoprene}) + MW_{TBDMS\text{-}Ade\text{-}AMA\text{-}SG1} - MW_{SG1} - MW_{TBDMS} + MW_{TEMPO\text{-}mal}$ with $DP_{n,NMR}$ calculated from ratio of areas under the peak at 8.69, 8.31 and 5.98 ppm (aromatic and anomeric proton of Ade) and 5.0–5.5 ppm (vinylic H in isoprene repeat unit (1,4-addition), corresponding to ~ 81% of total isoprene units [37]). $M_{n,SEC}$ = 5390 g mol^{-1}, $M_{n,NMR}$ = 7230 g mol^{-1}, $Đ$ = 1.37. mal/Ade = 0.63.

Synthesis of Ade-PI-Rho. Briefly, Ade-PI (0.300 g, 0.048 mmol, 1 eq) and TEMPO-Rho (0.038 g, 0.048 mmol, 1 eq) were placed in a 7 mL-vial and dissolved in 1 mL of dry pyridine. After 20 min of degassing under argon, the vial was placed in a preheated oil bath at 110 °C and stirred for 16 h. **Ade-PI-Rho** was then precipitated two times in cold methanol and dried under reduced pressure until constant weight. The post-functionalization yield was calculated by ^{1}H NMR using the chemical shifts of aromatic protons of Rho (δ = 7.70, 7.55, 7.08 and 6.93–6.67 ppm) and the chemical shifts of aromatic protons and anomeric proton of Ade (δ = 8.69, 8.31 and 5.98 ppm). Functionalization was confirmed by SEC equipped with a fluorescent detector (λ_{ex} = 570 nm, λ_{em} = 595 nm). $M_{n,NMR}$ was calculated according to $M_{n,NMR} = (DP_{n,NMR} \times MW_{isoprene}) + MW_{TBDMS\text{-}Ade\text{-}AMA\text{-}SG1} - MW_{SG1} - MW_{TBDMS} + MW_{TEMPO\text{-}Rho}$ with $DP_{n,NMR}$ calculated from ratio of areas under the peak at 8.69, 8.31 and 5.98 ppm (aromatic and anomeric proton of Ade) and 5.0–5.5 ppm (vinylic H in isoprene repeat unit (1,4-addition), corresponding to ~ 81% of total isoprene units [37]). $M_{n,SEC}$ = 7540 g mol^{-1}, $M_{n,NMR}$ = 6120 g mol^{-1}, $Đ$ = 1.32. Rho/Ade = 0.94

2.4. Nanoparticle preparation

PI (PI3), **Ade-PI, PI-mal** and **Ade-PI-mal** NPs were prepared by the nanoprecipitation technique [45]. All NPs were obtained by co-nanoprecipitation of the desired polymer with a Rho-containing PI to reach 5 wt% of Rho moieties with respect to the overall weight of NPs, as

follows: **Ade-PI-Rho/Ade-PI**, **Ade-PI-Rho/Ade-PI-mal**, **PI-Rho/PI** and **PI-Rho/PI-mal**. This percentage gave the best compromise in terms of fluorescence signal and NP colloidal characteristics (e.g., average size, stability). Briefly, 2.5 mg of the corresponding polymers were dissolved in 0.5 mL of THF and the solution was quickly added to 1 mL MilliQ water·THF was evaporated at r.t. using a Rotavapor. Intensity-averaged diameter (D_z) in MilliQ water and zeta potential measurements in 1 mM NaCl were carried out in triplicate by DLS. Their colloidal stability was assessed in water for 14 days. NPs were stored at 4 °C and allowed to reach r.t. before each measurement. To establish the best conditions for protein functionalization, **PI** and **Ade-PI** NP colloidal stability was tested following incubation at r.t. overnight and at 37 °C for 30 min, in either PBS or hCMEC/D3 cell medium without serum (which is important to avoid coating with serum proteins).

2.5. hCMEC/D3 cell culture

Immortalized human cerebral microvascular endothelial cells (hCMEC/D3) cells were used as a well-established model of the BBB that forms tight junctions (TJs), the major mechanism that prevents passage of most biomolecules and pharmacological agents from the blood to the brain [3,48–50]. Briefly, hCMEC/D3 cells were seeded (60.000 cells cm^{-2}) between passages 25 and 35 on the apical side of transwell filters coated with rat-tail collagen type I (4 μg cm^{-2}). Cells were grown for 14 days in EBM-2 medium supplemented with fetal bovine serum (5%), hydrocortisone (1.4 μM), HEPES (10 mM), penicillin-streptomycin (1%), basic fibroblast growth factor (1 ng mL^{-1}), ascorbic acid (5 μg mL^{-1}), and lipid concentrate (1/100). Medium was changed every 2–3 days (500 μL in the apical compartment, 1 mL in the basolateral compartment). Trans-endothelial electrical resistance (TEER) was measured every day to monitor the formation of tight junctions (EVOM2, World Precision Instruments), and was also measured in the presence of NPs (0.1 mg mL^{-1} added to the apical compartment for 3 h at 37 °C) and medium with no serum. Integrity of tight junctions was assessed by measuring the paracellular permeability of lucifer yellow (LY) across hCMEC/D3 monolayer. Briefly, LY (50 μM in PBS) was added to the apical compartment of the transwell system for 60 min. Every 30 min, samples were collected from the basolateral compartment. Quantification of fluorescence (λ_{ex} = 425 nm, λ_{em} = 530 nm) was carried out using a spectrofluorimeter (Perkin Elmer, LS50 B). The apparent permeability coefficient (Papp) for LY was calculated as previously described [51]. Permeability of FITC-dextran (40 kDa) was assessed after incubating cells in transwells with medium supplemented with either 0% or 5% serum for 24 h. All medium was removed, and FITC-dextran was added to the apical compartment (1 mg mL^{-1} in PBS), with 1 mL serum-depleted medium in the basolateral compartment. After 3 h incubation, fluorescence spectroscopy was used to quantify FITC-dextran in both compartments, and endothelial permeability was calculated [51].

2.6. Cell viability in the presence of polymer NPs

The viability of hCMEC/D3 cells after exposure to medium with no serum or NPs for 3 h at 37 °C was assessed using the MTT assay, as previously described [52]. Four types of bare NPs were used, each labelled with 5% wt. Rho: PI (**PI**), Ade-PI (**Ade-PI**), PI-mal (**PI-mal**) and Ade-PI-mal (**Ade-PI-mal**).

2.7. NP functionalization with physiological proteins and protein corona formation

Protein functionalization. 100 μL of **PI** and **Ade-PI** NPs (for adsorption) or **PI-mal** and **Ade-PI-mal** NPs (for covalent conjugation) at 2.5 mg mL^{-1} were incubated with 400 μL of one of the proteins ($MW_{Fet\ A}$ = 49 kDa, $MW_{\alpha 2M}$ = 180 kDa and MW_{BSA} = 66 kDa; 1.25 mg mL^{-1}) in hCMEC/D3 serum-free cell medium overnight at r.t., under which conditions the NPs were stable, as determined by previous stability tests. Free proteins were separated from NP-protein complexes by ultrafiltration (MWCO 300 kDA) at r.t. for 3 min at 14,000 *g*. NPs were resuspended in serum-free medium, and BCA assay (Thermo Fischer Scientific) was used to determine protein binding.

Protein corona formation. To test potential size changes upon protein corona formation, 25 μL bare, protein-adsorbed or protein-conjugated NPs (62.5 μg) were incubated in 200 μL cell medium containing 5% FBS for 30 min at 37 °C. Unbound proteins were removed by ultrafiltration (MWCO 300 kDA) for 6 min at 14,000 *g*. NPs were resuspended in MilliQ water and size was measured by DLS.

Assessment of protein covalent binding. To establish whether proteins can covalently bind to the maleimide moieties present on the polymeric NPs, Ellman's protocol was used to determine free thiol groups [53,54]. **PI**, **Ade-PI, PI-mal** and **Ade-PI-mal** NPs (50 μg) were incubated with each protein (150 μg) in 500 μL serum-free medium overnight at r.t., and free protein was removed by ultrafiltration as before. 5 μL of Ellman's reagent (2 mM DTNB in 50 mM sodium acetate) was added to NP-protein samples diluted 1:15 in PBS (final volume 150 μL) in 96 well plates. Plate was shaken and incubated at r.t. for 5 min. Optical absorbance was measured at 412 nm. A standard curve was created using known amounts of *N*-acetyl-L-cysteine, and nmol of free cysteine per mg protein was calculated. All samples were measured in triplicate and experiments were repeated three times.

2.8. Endothelial permeability and cellular uptake of NPs in an in vitro model of the healthy BBB

On the 14th day after cell seeding in the transwell system, 0.1 mg mL^{-1} of bare, protein-adsorbed or protein-conjugated NPs (determined to be non-toxic by MTT assay) suspended in 500 μL serum-free medium were added to the apical "blood" compartment of the transwell for 3 h at 37 °C. Note that the use of serum-free cell medium has already been utilized for similar NP permeability studies using this cell model [46,47]. Also, cell viability (MTT), permeability (TEER and EP after incubation with FITC-dextran, M_W = 40 kDa) were tested using serum-free medium and there was no effect on hCMEC/D3 permeability and viability after 3 h incubation. The basolateral "brain" compartment contained 1 mL of serum-free medium. At different time points for up to 3 h, an aliquot from the basolateral compartment was collected and fluorescence of Rho was measured using a spectrofluorimeter (Perkin Elmer, LS50 B). Excitation was set at 555 nm, and emission at 578 nm for **PI** and **PI-mal** NPs or 587 nm for **Ade-PI** and **Ade-PI-mal** NPs. For each experiment, a standard curve was established using bare NPs of a known concentration that were not subjected to ultrafiltration. Each experiment used triplicate wells and was repeated at least three times. Transwell filters without cells were used as a control to calculate the endothelial permeability (EP) of NPs across the filter. EP takes into account passage of NPs through the transwell filter alone to give a value representative of the rate of passage through the cell monolayer, and was calculated as previously described [51].

To measure cellular uptake of NPs after 3 h incubation, cells were washed twice with Dulbeccos's PBS (DPBS) and incubated with 0.25% trypsin-EDTA for 5 min at 37 °C. Control wells without cells were used to rule out NPs adherence to the filter. Trypsinized cells were collected and centrifuged at 2000 rpm (1500 g) for 5 min. Supernatant was discarded and the pellet of cells was resuspended in 750 μL cold lysis buffer (50 mM Tris-HCl pH 7.4, 150 mM NaCl, 2 mM EDTA, 1% v/v Triton X-100, 0.1% SDS, 1 mM DTT). Cells were incubated for 30 min at r.t. while rotating in the dark and then centrifuged at 10,000 rpm (7500 g) for 5 min. The supernatant was collected and fluorescence was measured as above described. Cellular uptake was expressed as a percentage of the initial amount of NPs added to the apical compartment, subtracting the fluorescence measurements obtained from wells without cells.

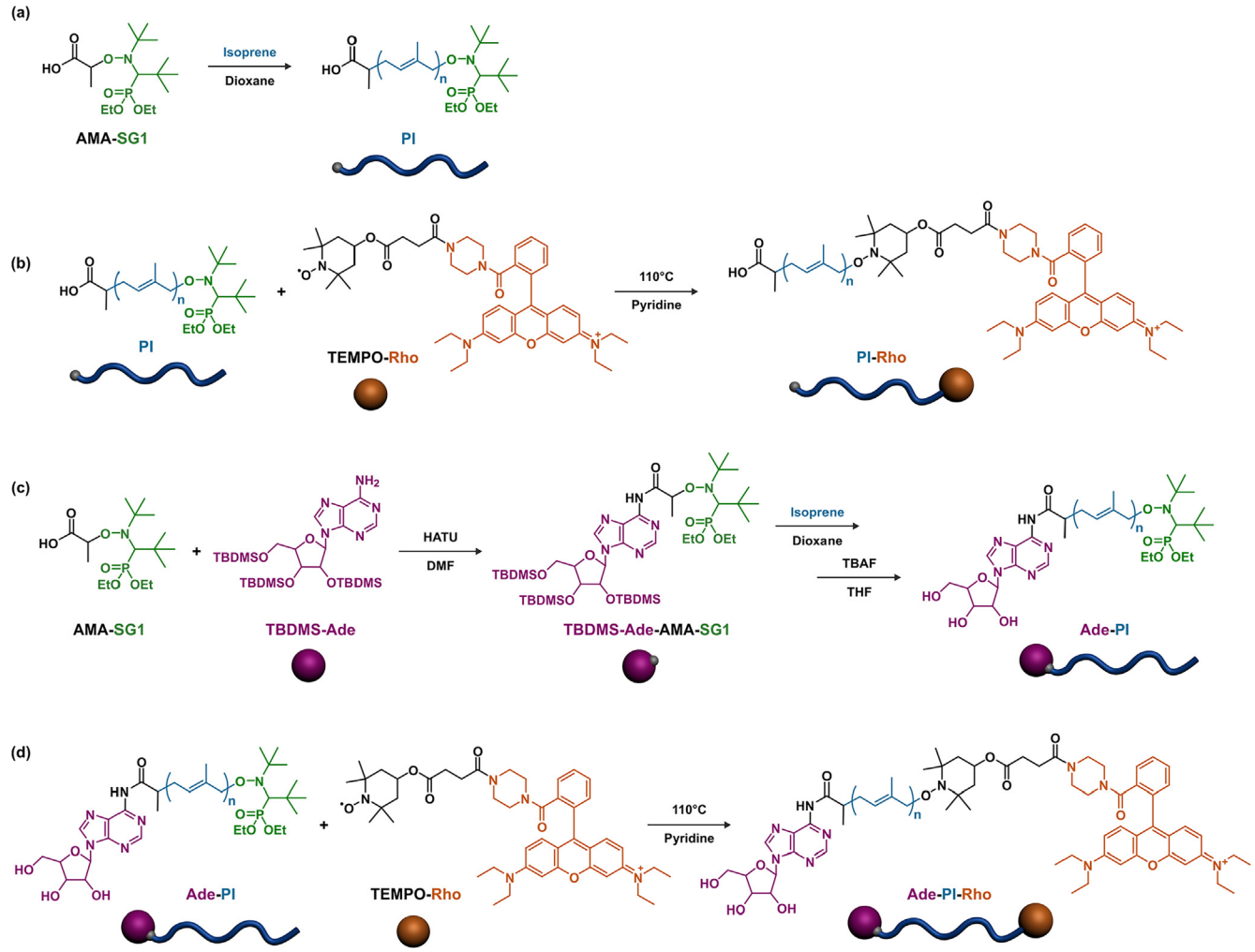

Scheme 1. (a) Synthesis of polyisoprene (**PI**) by nitroxide-mediated polymerization (NMP) initiated by the AMA-SG1 alkoxyamine. (b) Synthesis of PI-rhodamine (**PI-Rho**) by the nitroxide exchange reaction with TEMPO-rhodamine (TEMPO-Rho) on **PI**. (c) Synthesis of adenosine-polyisoprene (**Ade-PI**) by NMP of isoprene from tris-O-silylated-adenosine-AMA-SG1 alkoxyamine (TBDMS-Ade-AMA-SG1), followed by deprotection of Ade. (d) Synthesis of adenosine-polyisoprene-rhodamine (**Ade-PI-Rho**) by the nitroxide exchange reaction with TEMPO-rhodamine (TEMPO-Rho) on **Ade-PI**.

2.9. Visualization of cellular uptake of NPs by hCMEC/D3 cells using fluorescence microscopy

hCMEC/D3 cells were seeded on rat collagen type I-coated Cell Carrier Ultra 96 well plates (10,000 cells/well) and grown for two days. When cells were confluent, they were incubated with 100 µL bare **PI**, **Ade-PI**, **PI-mal** and **Ade-PI-mal** NPs in serum-free cell medium (0.1 mg mL^{-1}) for 3 h at 37 °C. NPs were then removed from the wells and cells were washed twice with DPBS. Cells were fixed with 10% formalin solution (100 µL) at r.t. for 20 min, followed by three 10 min washes with DPBS. Cells were permeabilized with 100 µL Triton (0.2% v/v) for 15 min at r.t. and washed once with DPBS. The actin cytoskeleton was stained with Phalloidin Alexafluor 633 (1:100 in DPBS) for 1 h at r.t., and then washed 3 times with DPBS. Hoescht (1:5000 in DPBS) was incubated for 15 min at r.t. to stain nuclei. Cells were washed three times in DPBS and all wells were filled with MilliQ water (100 µL). Plates were stored in the dark at 4 °C until visualization. Fluorescent microscopy images were acquired using the Operetta CLS High-Content Analysis System (PerkinElmer) equipped with 40x water objective. Excitation of NPs was set to 530–560 nm, emission at 570–650 nm.

3. Results and discussion

3.1. Overall synthetic strategy

Heterotelechelic polymers were synthesized by the "*drug-initiated*" method [55]. It relies on the controlled growth of a polymer chain from a drug covalently linked to an "initiator" using reversible-deactivation radical polymerization (RDRP) techniques, especially nitroxide-mediated polymerization (NMP) [42,56–59] and reversible addition-fragmentation chain transfer polymerization (RAFT) [59–64]. This synthetic approach has key advantages: (i) purification of the drug-polymer prodrug is simplified as only unreacted monomer has to be removed; (ii) the conjugation of the drug is quantitative, leading to well-defined conjugates with one drug molecule attached to each polymer chain and (iii) the drug loading (DL) can be fine-tuned by varying the polymer chain length; the lower the chain-length, the higher the DL. Polyisoprene (PI) was selected as the polymer for its biocompatibility [65] and structural similarity to natural terpenoids, hence representing a potential material for drug delivery applications [38,42,57,59].

To functionalize the other polymer chain-end and obtain heterotelechelic polymer prodrugs, we recently developed a general and robust methodology consisting of applying a nitroxide-exchange reaction to "*drug-initiated*" synthesized polymers obtained by NMP [38,66]. The

terminal SG1 nitroxide was quantitatively replaced by a functional TEMPO nitroxide bearing the molecule of interest, which was either a fluorescent probe for imaging applications or a second drug for combination therapy. This methodology has important benefits such as nearly quantitative post-functionalization yields and easy purification given the absence of any catalyst or reactant other than the free nitroxide and the polymer. Also, TEMPO can be functionalized by a variety of different moieties at the 4-position.

To allow NP surface functionalization with cysteine-containing proteins, the TEMPO nitroxide was derivatized by a protected maleimide group [67–69]. TEMPO was also functionalized with a Rho moiety to endow NPs with fluorescence properties by a simple co-nanoprecipitation approach. Rho was chosen as a fluorescent probe because of its favorable characteristics such as good photostability, high quantum yield, high extinction coefficient and higher emission wavelengths than those coming from cell autofluorescence [70]. Rho was also previously modified with a piperazine ring to avoid intramolecular cyclization and allow good stability with pH modifications [71]. The covalent linkage of Rho to the polymer, as opposed to simple encapsulation, is intended to avoid potential leakage of the dye, which could result in the detection of artifact coming from the free dye by fluorescence spectroscopy [38,58].

3.2. Synthesis of heterotelechelic polymer prodrug

PI was synthesized from AMA-SG1 alkoxyamine initiator (Scheme 1a) with M_n ranging from 2860 to 4940 g mol^{-1} and low dispersity (1.13–1.18, Table 1). **PI-Rho** was obtained by nitroxide exchange reaction from **PI** and TEMPO-Rho (Scheme 1b and Table 1). Unfortunately, it was not possible to calculate the post-functionalization yield by 1H NMR because of the lack of a suitable proton in α position to be compared with those of Rho, but previous demonstration by electron spin resonance [38] and characterization of heterotelechelic polymers showed below, led us to assume it was quasi-quantitative.

As for Ade-PI (Scheme 1c), Ade hydroxyl groups were first protected by TBDMS and the resulting TBDMS-Ade was covalently linked to AMA-SG1 alkoxyamine initiator by HATU coupling to give TBDMS-Ade-AMA-SG1 (62% overall yield). By varying the experimental conditions, it then served as an initiator for the NMP of isoprene to yield well-defined **TBDMS-Ade-PI** (see experimental part) with $M_{n,SEC} \sim 5500$ g mol^{-1} and $Đ = 1.16$. After deprotection in the presence of TBAF, **Ade-PI** was obtained. The effectiveness of the reaction was confirmed by ^{1}H NMR, which showed the disappearance of the silylated protecting groups (Fig. S1) and a slight decrease of the $M_{n,NMR}$ because of TBDMS group removal (see experimental part and Table 1).

Post-functionalization by nitroxide exchange reaction was performed on **Ade-PI** in presence of 1 eq. of TEMPO-Rho to yield **Ade-PI-Rho** as a fluorescent heterotelechelic polymer prodrug (Scheme 1d and Table 1). **Ade-PI-Rho** was characterized by ^{1}H NMR spectroscopy and gave the expected structure. Rho aromatic protons were detected in the 6.5–8 ppm region, together with those from the piperazine ring in the 4–4.5 ppm region (Fig. S2). Complete disappearance of SG1 protons in the 3.2–3.4 ppm region was also observed. Integration of aromatic proton signals of Ade and Rho gave a nearly quantitative post-functionalization yield as the Rho/Ade molar ratio was as high as 94 mol.% (Table 1). SEC equipped with a fluorescent detector revealed comparable molar mass distribution profiles for both RI and fluorescence traces, supporting a uniform end-capping process by TEMPO-Rho (Fig. S3a). Moreover, RI traces between **Ade-PI** and **Ade-PI-Rho** were almost perfectly overlaid, indicating negligible irreversible termination by recombination (Fig. S3b).

To allow NP surface functionalization with BBB-targeting proteins by covalent linkage, a maleimide moiety was installed at the ω-chain end of **PI** and **Ade-PI** through the nitroxide exchange reaction. However, direct nitroxide exchange from a TEMPO bearing a furan-protected maleimide group led to extensive occurrence of termination reactions and doubling of the starting M_n (Fig. S4), likely because of *in situ* deprotection of the maleimide group at elevated temperature and radical addition onto it. The furan-protected maleimide was therefore introduced in a two-step process, by first performing the nitroxide exchange reaction with 4-hydroxy-TEMPO, followed by coupling with a succinate furan-protected maleimide (succinic-mal-furan, Scheme 2a). **PI-mal** was also prepared by subjecting **PI** to nitroxide exchange in the presence of 4-hydroxyl-TEMPO to give **PI-OH.** After coupling with succinic-mal-furan under EDC assistance to give **PI-mal-furan**, **PI-mal** was recovered after maleimide deprotection (see experimental part, Scheme 2b and Table 1). SEC analysis did not show noticeable changes in molar mass distributions and ^{1}H NMR confirmed the presence of maleimide and disappearance of SG1 protons. Even though absence of a suitable proton in α-position prevented determination of the coupling yield, it was expected to be very similar to **Ade-PI-mal**.

A furan-protected maleimide derivative was reacted with succinic anhydride to give succinic-mal-furan with a 96% yield (Scheme 2a), meanwhile the nitroxide exchange reaction was performed on **TBDMS-Ade-PI** with 4-hydroxy-TEMPO to give **TBDMS-Ade-PI-OH** (Scheme 2b and Fig. S5). Even though absence of visible protons peaks on TEMPO prevented calculation of the nitroxide exchange yield by ^{1}H NMR, disappearance of SG1 protons (Fig. S6) and the previous successful use of this reaction [38] indicates that it was quantitative. Subsequent coupling between **TBDMS-Ade-PI-OH** and a furan-protected maleimide assisted by EDC yielded the expected **TBDMS-Ade-PI-mal-furan**. The post-functionalization yield was calculated by comparing Ade aromatic and anomeric protons (δ = 6.53, 4.22, 2.90 ppm) and the maleimide proton (δ = 2.68 ppm), and reached 60% (Fig. S5, experimental part). Ade was then deprotected with TBAF followed by maleimide deprotection in toluene at 100 °C to give **Ade-PI-mal** (Table 1). Complete disappearance of both protecting groups, appearance of a signal corresponding to maleimide protons at 7.14 ppm, and shift of Ade anomeric proton from 6.10 to 6.24 ppm (likely due to a change of the chemical environment), confirmed the effectiveness of the deprotections (Fig. S6). All polymers were also characterized by SEC and showed good conservation of the macromolecular characteristics throughout

Table 1
Characterization of Polyisoprene (PI), Polyisoprene-Rhodamine (PI-Rho), Adenosine-Polyisoprene (Ade-PI), Adenosine-Polyisoprene-Rhodamine (Ade-PI-Rho), Adenosine-Polyisoprene-Maleimide (Ade-PI-mal) and Polyisoprene-Maleimide (PI-mal).

Prodrug	$M_{n,SEC}$[a] (g mol^{-1})	$Đ$[a]	$M_{n,NMR}$ (g mol^{-1})	$DP_{n,NMR}$[e]	Rho or mal/Ade[f]	Drug loading (wt.%) [g]
PI	2860	1.13	–	–	–	–
PI-Rho	2690	1.13	–	–	–	–
Ade-PI	6260	1.15	6280[b]	83	–	4.3
Ade-PI-Rho	7540	1.32	6120[c]	74	0.94	3.5
Ade-PI-mal	5390	1.37	7230[d]	95	0.63	5.0
PI-mal	5650	1.17	–	–	–	–

[a] Determined by SEC, calibrated with PS standards and converted into PI by using Mark-Houwink-Sakurada parameters.

[b] Calculated according to $M_{n,NMR} = (DP_{n,NMR} \times MW_{isoprene}) + MW_{TBDMS\text{-}Ade\text{-}AMA\text{-}SG1} - MW_{TBDMS}$

[c] Calculated according to $M_{n,NMR} = (DP_{n,NMR} \times MW_{isoprene}) + MW_{TBDMS\text{-}Ade\text{-}AMA\text{-}SG1} - MW_{SG1} - MW_{TBDMS} + MW_{TEMPO\text{-}Rho}$.

[d] Calculated according to $M_{n,NMR} = (DP_{n,NMR} \times MW_{isoprene}) + MW_{TBDMS\text{-}Ade\text{-}AMA\text{-}SG1} - MW_{SG1} - MW_{TBDMS} + MW_{TEMPO\text{-}mal}$.

[e] Calculated from ratio of areas under the peak at 8.69, 8.31 and 5.98 ppm (aromatic and anomeric proton of Ade) and 5.0–5.5 ppm (vinylic H in isoprene repeat unit (1,4-addition), corresponding to ~ 81% of total isoprene units [37]).

[f] Calculated from ratio of areas under the peak of aromatic protons of Rho at 7.70, 7.55, 7.08 (or of mal at 6.53, 4.22, 2.90 and 2.68 ppm) and 6.93–6.67 ppm and aromatic and anomeric protons of Ade at 8.69, 8.31 and 5.98 ppm.

[g] Calculated according to $MW_{Ade}/M_{n,SEC}$.

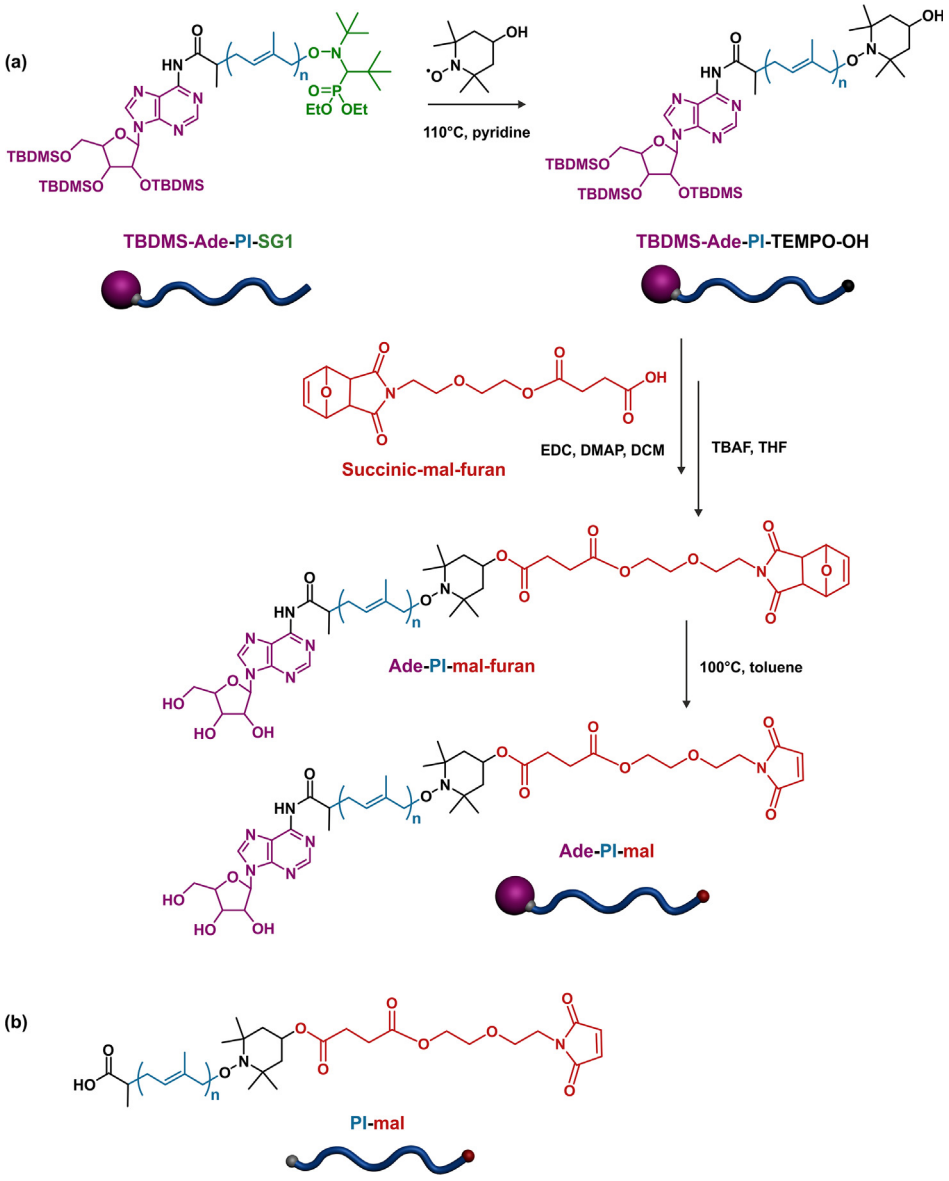

Scheme 2. (a) Synthesis of adenosine-polyisoprene-maleimide (**Ade-PI-mal**) by nitroxide-mediated polymerization (NMP) of isoprene from tris-O-silylated-adenosine-AMA-SG1 alkoxyamine (TBDMS-Ade-AMA-SG1), followed by the nitroxide exchange with 4-hydroxy-TEMPO on TBDMS-Ade-AMA-SG1, EDC-assisted functionalization by succinic-mal-furan and subsequent deprotections of Ade and maleimide. (b) Structure of **PI-mal** obtained by the nitroxide exchange with 4-hydroxy-TEMPO on PI, EDC-assisted functionalization by succinic-mal-furan and subsequent deprotection of maleimide.

the different steps (Fig. S7, experimental part).

In summary, six different polymers were synthesized (Table 1): (i) two Ade prodrug polymers, bearing a maleimide group (**Ade-PI-mal**) or not (**Ade-PI**); (ii) two Ade-free polymers, bearing a maleimide group (**PI-mal**) or not (**PI**) and (iii) two fluorescent polymers, bearing Ade (**Ade-PI-Rho**) or not (**PI-Rho**).

3.3. NP formulation and colloidal characteristics

The previously synthesized polymers were formulated into NPs in order to compare bare (i.e., protein-free) NPs to NPs functionalized with BBB-targeting proteins, either by adsorption or conjugation, and to investigate the influence of the drug on NP colloidal properties. Drug loading of the different polymer prodrugs ranged from 3.5 to 5 wt%, depending on the M_n of the polymer (Table 1). It is worth noting that higher drug loading values could be easily obtained by targeting lower molar mass polymers. Here, a relatively high M_n was targeted to increase NP surface hydrophobicity, which is known to increase protein affinity towards the NP surface [72,73].

Four different types of NPs were formulated by the nanoprecipitation technique at a concentration of 2.5 mg mL^{-1}: drug-free NPs (**PI**) and polymer prodrug NPs (**Ade-PI**) for protein adsorption or drug-free NPs containing maleimide groups (**PI-mal**) and polymer prodrug NPs containing maleimide groups (**Ade-PI-mal**) for protein conjugation (Table 2). All NPs were also fluorescently-tagged by co-nanoprecipitation with **PI-Rho** or **Ade-PI-Rho** (5 wt% Rho) to confer fluorescent properties and allow tracing during biological evaluations.

NPs were very similar in terms of average size (D_z = 162–185 nm) and had low particle size distribution (PSD) values varying from 0.10 to 0.21. Whereas zeta potential of PI-based prodrug NPs is usually strongly negative [42,57], all NPs here had a strong positive zeta potential value, between + 40 and + 50 mV. This is due to the presence of positive charges on the Rho molecule, as already observed for other PI NPs labeled with this fluorophore [38]. In addition to the nanoparticle surface hydrophobicity provided by the polymer, the positive charge from Rho could also increase the NP affinity towards the proteins used

Table 2
Colloidal Characteristics of NPs Prepared by Co-nanoprecipitation of PI, Ade-PI, PI-mal or Ade-PI-mal with PI-Rho or Ade-PI-Rho (5 wt% Rho).

Sample	D_z [a] (nm)	PSD [a]	ζ [a] (mV)
PI [b]	185 ± 1	0.13 ± 0.001	49 ± 2
Ade-PI [c]	179 ± 3	0.11 ± 0.03	45 ± 1
PI-mal [b]	164 ± 14	0.21 ± 0.01	41 ± 15
Ade-PI-mal [c]	162 ± 3	0.10 ± 0.02	50 ± 4

[a] Measured by dynamic light scattering (DLS) as an average of three different measures.
[b] Co-nanoprecipitated with PI-Rho (5 wt% Rho).
[c] Co-nanoprecipitated with Ade-PI-Rho (5 wt% Rho).

for functionalization [74–78]. Note that Rho has been extensively used for NP and peptide labelling in cell uptake/permeability studies, but the positive charge of the Rho alone has not been enough to dictate the cell-NP interactions [79].

NP colloidal stability was assessed in water and they were all stable for at least 14 days (Fig. 2a). To optimize protein functionalization conditions, **PI** and **Ade-PI** colloidal stability was also tested in PBS and hCMEC/D3 cell culture medium without serum at r.t., at 4 °C overnight, or at 37 °C for 30 min (Fig. 2b and c). The hCMEC/D3 immortalized human brain endothelial cell line is a widely used model of the BBB, forming the characteristic tight junctions, architectural structure, and protein expression found in the human barrier [80]. NPs were stable in cell medium but aggregated in PBS, therefore the former was used in further experiments.

3.4. Coating and functionalization of NPs with BBB crossing proteins

We recently found that specific proteins are enriched in the protein corona of gold NPs following passage through a transwell model of the BBB [48], emphasizing their potential ability to reach the brain after *in vivo* administration. It was postulated that the formation of an artificial corona consisting of one of these specific proteins could enhance the passage of NPs through the BBB.

The presence of maleimide on the polymer should allow covalent binding of NPs with proteins that have a free cysteine residue. BSA [81], α2M [82] and Fet A [83] have cysteine residues at different oxidation states that could be theoretically available for covalent binding to **PI-mal** and **Ade-PI-mal** NPs. Moreover, given the strongly positive NP surface charge (Table 2), simple adsorption of the proteins was also investigated, as it has been extensively shown that a wide array of proteins are easily adsorbed *via* strong electrostatic interactions with the surface of NPs [84]. However, there are several advantages of choosing covalent binding over the simple adsorption of proteins on the surface of NPs, including improved selectivity of protein binding. Furthermore, as covalent bonds are stronger than electrostatic forces, this may possibly prevent the displacement of functionalized proteins by serum proteins upon *in vivo* administration, or their removal in the purification process [85].

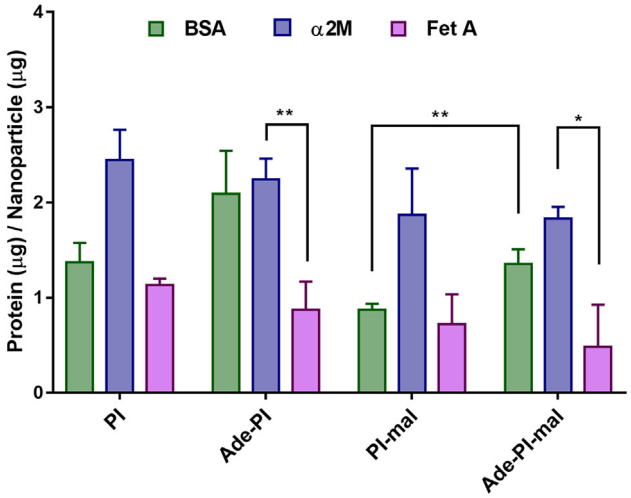

Fig. 3. Amount of protein bound to NPs (μg protein/μg NP), as measured by BCA assay after incubation of NPs with protein in serum-free cell medium overnight at r.t., followed by ultrafiltration to remove unbound protein (n = 3, error bars represent SEM. Student's *t* test * $p < 0.05$, ** $p < 0.01$).

NPs were incubated overnight at r.t. with each protein suspended in hCMEC/D3 cell medium without serum, to avoid serum protein interferences, then ultrafiltrated to remove unbound protein. BCA quantification indicated that the highest amount of protein binding occurred with α2M on all NPs (1.8–2.4 μg protein/μg NP) and the lowest with Fet A (0.5–1.1 μg protein/μg NP), possibly due to differences in MW as $MW_{\alpha 2M}$ = 180 kDa and $MW_{Fet\ A}$ = 49 kDa (Fig. 3). The presence of Ade

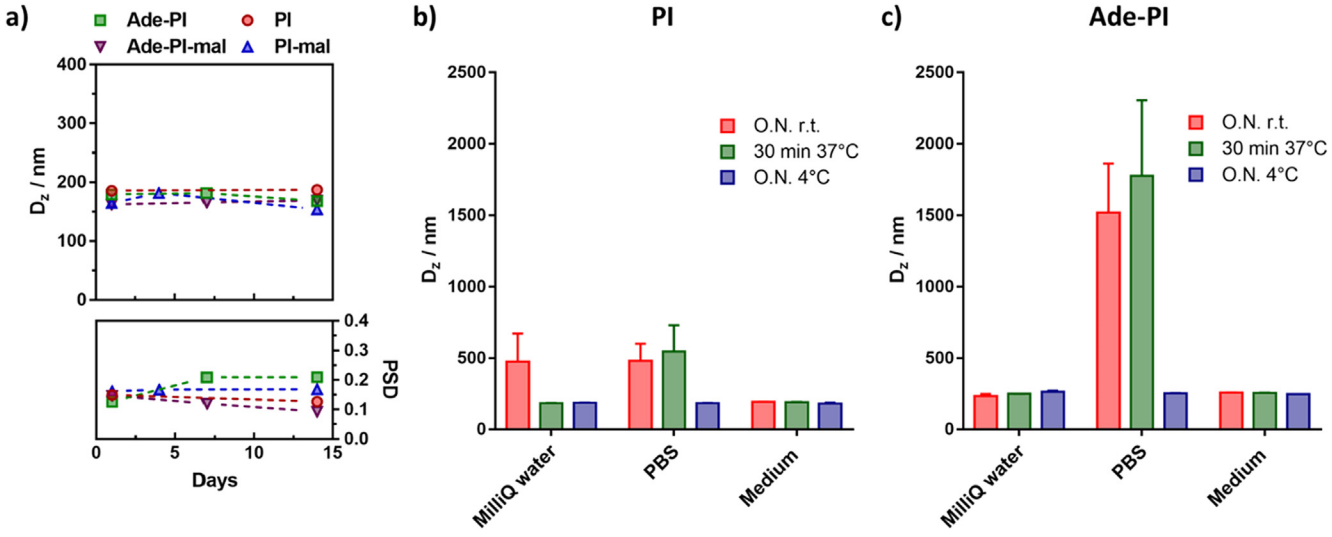

Fig. 2. (a) Evolution of the intensity-averaged diameters (D_z) and particle size distributions (PSD) in water of Ade-PI, PI, Ade-PI-mal and PI-mal NPs blended with PI-Rho or Ade-PI-Rho (5 wt%. Rho) measured by DLS over 14 days. Stability in milliQ water, PBS and cell culture medium without serum incubated overnight (O.N.) at room temperature (r.t.), O.N. at 4 °C, or for 30 min at 37 °C of (b) **PI** or (c) **Ade-PI**. NPs at 0.1 mg mL^{-1} in order to determine the best conditions for protein functionalization (n = 3, error bars represent SEM).

significantly increased BSA binding in the presence of mal (1.4 μg protein/μg NPs on **Ade-PI-mal** vs 0.9 μg protein/μg NPs on **PI-mal**) but did not significantly affect α2M or Fet A binding.

To confirm that proteins could covalently bind to maleimide moieties present on the NPs and to discriminate between adsorbed and covalently linked proteins, Ellman's protocol was used to determine free thiol groups [53,54]. If a NP is covalently bound to a protein, the number of free thiols present on the protein should decrease, as the thiol groups are attached to the maleimide moiety. Ellman's reagent was used to quantify free cysteine on BSA, α2M or Fet A following incubation with either **PI**, **PI-mal**, **Ade-PI** or **Ade-PI-mal** NPs (Fig. S8). For all proteins, there was significantly less free cysteine following incubation with **PI-mal** and **Ade-PI-mal** NPs compared to incubation with **PI** and **Ade-PI** NPs respectively, indicating that covalent binding occurred in the presence of maleimide. Even though there is likely a mix of adsorbed/linked proteins at the surface of **PI-mal** and **Ade-PI-mal** NPs, their total amount was not significantly different to that of only adsorbed proteins at the surface of **PI** and **Ade-PI** NPs.

Further confirmation of successful protein functionalization was obtained by measuring the hydrodynamic diameter of NPs. It has been previously shown that NPs increase in size upon protein functionalization and protein corona formation [86]. Therefore, the size of NPs with or without protein functionalization was also measured after incubation in serum to form a corona, and subsequent ultrafiltration to remove excess unbound serum proteins. For all NPs, both protein functionalization and protein corona formation resulted in a significant increase in size, with the latter causing a more dramatic increase (Fig. 4). The size increase upon corona formation is likely due to the adherence of multiple protein layers, containing proteins of diverse size bound directly to the NP surface and to each other. In the case of almost every NP-protein combination, prior protein functionalization prevented corona-associated size increases, and the size was comparable or identical to protein-functionalized NPs not exposed to serum. This is indicative of functionalization stability. Notably the ultrafiltration process itself caused a slight increase in **PI** (+36 nm), **PI-mal** (+23 nm), and **Ade-PI-mal** (+9 nm) NPs without proteins, but PSD values remained comparable before and after ultrafiltration (Fig. S9). Indeed, the PSD values for most nanoparticle-protein or nanoparticle-serum complexes did not significantly change compared to bare NPs. This indicated that size changes are not due to aggregation of NPs upon protein exposure, and is in agreement with studies showing increases in NP size upon protein binding [53,87–89].

3.5. Cellular uptake and permeability of functionalized NPs through a transwell BBB model

The next step was to evaluate the influence of the nanoparticle surface coating/functionalization on the cellular uptake and permeability using an *in vitro* BBB model. A simple but well characterized and widely used model of the BBB was established by seeding hCMEC/D3 cells on transwell inserts separating an apical "blood" side from a basolateral "brain" side [3,48–50]. Average TEER values peaked at 149 ± 3 $\Omega.cm^{-2}$ on the 14th day after seeding and the paracellular permeability of LY, a probe used to evaluate the integrity of *in vitro* tight junctions, was 1.51 ± 0.03 × 10^{-3} $cm.min^{-1}$, indicating the formation of tight junctions [48,51]. MTT assay showed that none of the NPs affected hCMEC/D3 cell viability up to 0.1 $mg\,mL^{-1}$ after 3 h incubation (Fig. S10). Furthermore, TEER values remained unchanged upon incubation of hCMEC/D3 cells with **PI**, **PI-mal**, **Ade-PI**, or **Ade-PI-mal** NPs for at least 3 h (Fig. S11) during which time the NPs were stable, despite an increase in diameter (Table S2).

All four bare PI-based NPs were internalized to some extent by hCMEC/D3 cells, as visualized by fluorescent microscopy (Fig. 5a) and quantified in the transwell model (Fig. 5b). Fluorescent microscopy showed that the NPs gathered in the perinuclear region of hCMEC/D3 cells after 3 h incubation, a pattern seen with other NPs and cell types

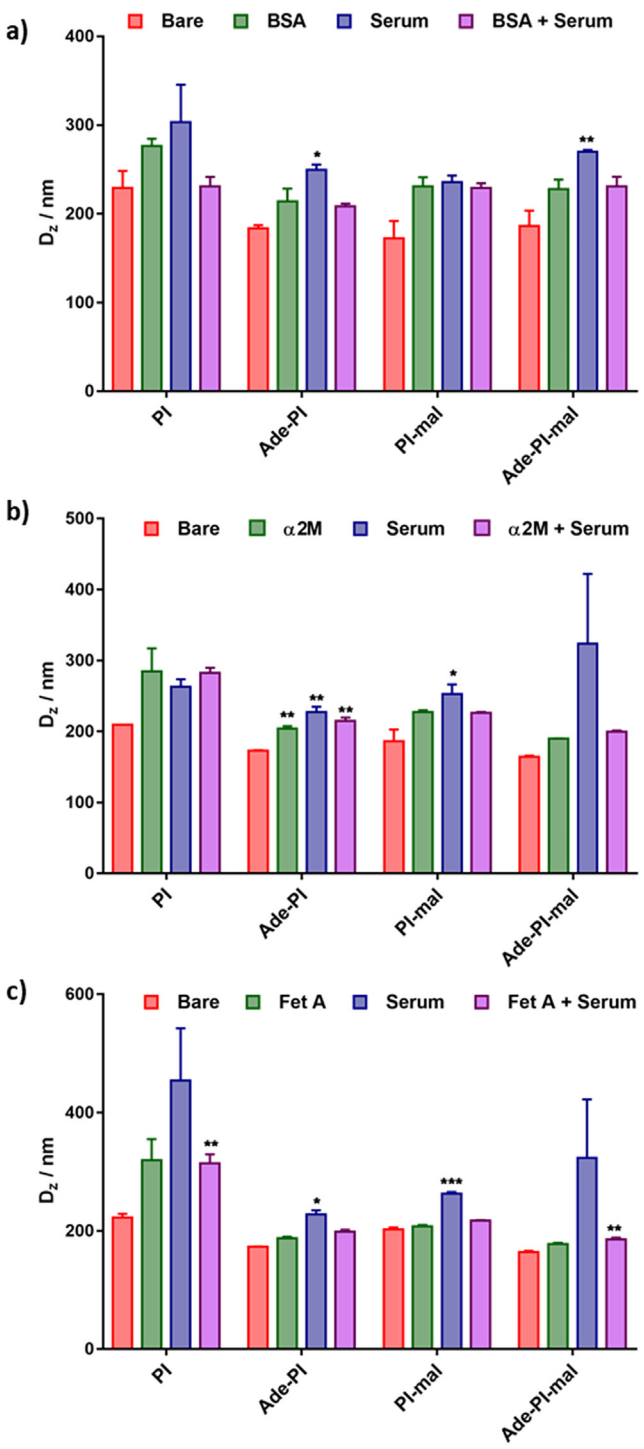

Fig. 4. Size of NPs upon protein functionalization and protein corona formation in serum, as measured by DLS after ultrafiltration to remove unbound proteins. Functionalization or coating of NPs with: (a) BSA, (b) α2M and (c) Fet A, with or without serum-derived protein corona (n = 3, error bars represent SEM. Statistical analysis (Student's *t* test) to compare size with bare NPs: * $p < 0.05$, ** $p < 0.01$, *** $p < 0.001$.

[90,91].

Remarkably, bare **PI** NPs, whose safety has already been demonstrated *in vivo* [42,57], had high cellular uptake (5.3 ± 0.8%) and endothelial permeability (EP) (9.5 × 10^{-4} $cm\,min^{-1}$) (Figs. 5b and 6). Compared to previously described bi-functionalized liposomes that can cross the BBB *in vitro* (EP = 2.5 × 10^{-5} $cm\,min^{-1}$) and *in vivo* [13], EP of **PI** NPs was ~ 4 times higher, which is likely due, at least partially, to

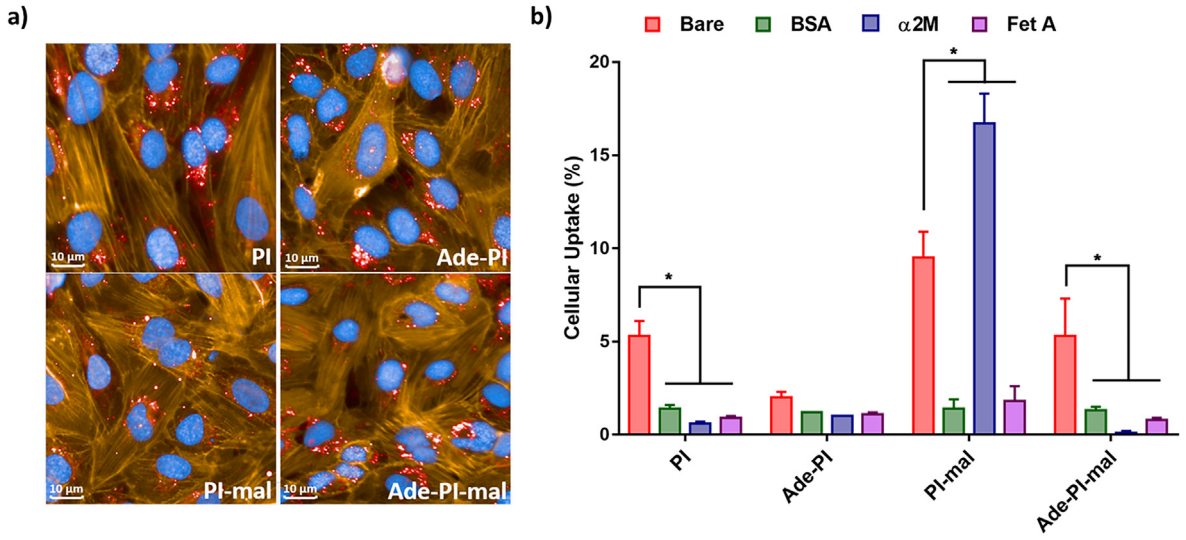

Fig. 5. Cellular uptake of **PI**, **Ade-PI**, **PI-mal** and **Ade-PI-mal** NPs in an *in vitro* BBB model. (a) Fluorescent microscopy images show localization of NPs in the perinuclear region of hCMEC/D3 endothelial cells after 3 h incubation at 37 °C. Orange staining is actin cytoskeleton, blue is cell nuclei, red is rhodamine labelled NPs; (b) Uptake of NPs by hCMEC/D3 cells, expressed as percentage of original NPs added to the apical side of the transwell (n = 3, error bars represent SEM, Student's *t* test $*p < 0.05$). (For interpretation of the references to colour in this figure legend, the reader is referred to the web version of this article.)

the high PI hydrophobicity, known to increase cellular uptake [57,92].

Importantly, the decrease in cell uptake observed upon protein functionalization of **PI** NPs (Fig. 5b) did not match with a decrease in permeability (Fig. 6). This indicates that the presence of proteins prevents the sequestering of NPs in the cell but may allow them to pass through the *in vitro* BBB at a similar or higher rate than bare **PI** NPs.

When considering **PI** and **PI-mal** NPs, the presence of maleimide moieties led to higher cellular uptake but a lower EP compared to **PI** NPs. However, covalently bound α2M at the surface of **PI-mal** NPs caused a significant increase in both cellular uptake and EP (Figs. 5b and 6). Therefore, this protein may be promising as a functionalization tool to promote passage of certain NPs through the BBB. Conversely, BSA and Fet A did not significantly affect the cellular uptake neither the EP of any of the PI-based NPs. This observation may be explained by differences in the packing/orientation of the proteins or alterations in protein conformation on the surface of NPs that may change protein-receptor interactions and subsequent cellular uptake [85,93,94].

Interestingly, the presence of Ade significantly decreased the endothelial permeability (EP) of NPs by ~ 4–8 fold when comparing **PI** and **Ade-PI** NPs, regardless of protein functionalization ($p < 0.01$) (Fig. 6). Given the relatively high water-solubility of Ade, many Ade moieties may be displayed at the surface of NPs, decreasing the NP surface hydrophobicity and thus modifying their interaction with proteins compared to **PI** NPs. This hypothesis is supported by the increase of the predicted HLB numbers for Ade-containing model prodrugs compared to Ade-free counterparts (Table S1). Similarly, **Ade-PI-mal** NPs had a lower cellular uptake than **PI-mal** NPs (5.3 ± 2.0% vs 9.5 ± 1.4%, $p < 0.05$), potentially due to a lower surface amount of reactive maleimide moieties caused by competition with hydrophilic Ade groups (Fig. 5b). This may explain why α2M did not significantly affect the EP of NPs with Ade.

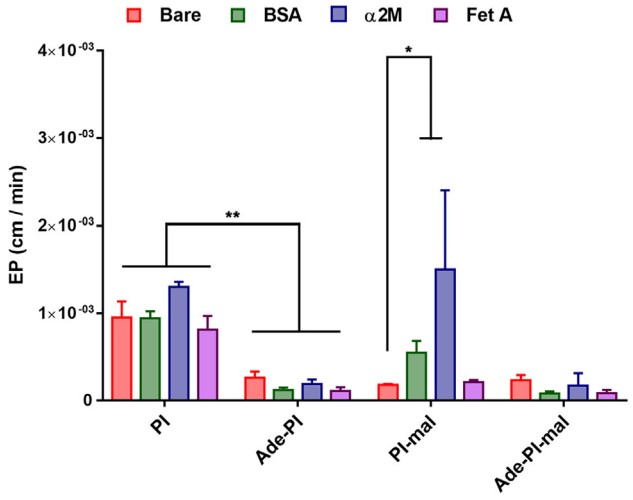

Fig. 6. Endothelial permeability (EP) of **PI**, **Ade-PI**, **PI-mal** and **Ade-PI-mal** NPs in an *in vitro* BBB model after 3 h at 37 °C (n ≥ 3, error bars represent SEM, Student's *t* test $*p < 0.05$, $**p < 0.01$).

4. Conclusion

Here we described a robust procedure for engineering well-defined, PI-based heterotelechelic polymer prodrug NPs for drug delivery and brain targeting. Heterotelechelic polymer prodrugs were prepared by the "*drug-initiated*" strategy followed by their post-functionalization via the nitroxide exchange reaction to position maleimide groups for conjugation of BBB-crossing proteins (BSA, α2M or Fet A) at the NP surface, as confirmed by Ellman's test and DLS measurements. All NPs were stable, with average diameters in the 162–185 nm range, narrow particle size distributions, and long-term colloidal stability in water and cell culture medium.

We showed that non-BBB-targeted PI-NPs already exhibit higher permeability and cellular uptake than targeted systems described in the literature, rendering this novel nanodevice highly attractive as a drug delivery system for brain-directed drugs or contrast agents. We also demonstrated that surface functionalization of these NPs with α2M enhanced their passage through an *in vitro* BBB model. This could be a promising BBB-targeting strategy *in vivo* that would warrant further investigation. Also, our results suggested that in case polymer-prodrugs are envisioned, the nature/solubility of the drug and/or its positioning within the NPs are crucial to achieve efficient surface functionalization with BBB-targeting proteins to enhance passage through the BBB.

Acknowledgements

This work was supported by the European Union's Horizon 2020 research and innovation programme under Marie Skłodowska Curie

grant agreement no. 642028 (NABBA). The authors thank Pierre-Olivier Couraud, Université Rene Descartes, for providing the hCMEC/D3 cells, and Stéphanie Nicolaÿ for mass spectrometry analyses (Service d'Analyses des Médicaments et Métabolites (Institut Paris-Sud d'Innovation Therapeutique (IPSIT)), Université Paris-Sud). Arkema is acknowledged for kindly providing the SG1 nitroxide. CNRS and Université Paris-Sud are also acknowledged for financial support.

Appendix A. Supplementary material

Supplementary data to this article can be found online at https://doi.org/10.1016/j.ejpb.2019.06.004.

References

[1] W.M. Pardridge, The blood-brain barrier: bottleneck in brain drug development, NeuroRX 2 (2005) 3–14.
[2] C. Saraiva, C. Praça, R. Ferreira, T. Santos, L. Ferreira, L. Bernardino, Nanoparticle-mediated brain drug delivery: overcoming blood–brain barrier to treat neurodegenerative diseases, J. Contr. Rel. 235 (2016) 34–47.
[3] R.D. Magro, A. Cox, V. Zambelli, S. Mancini, M. Masserini, F. Re, The ability of liposomes, tailored for blood–brain barrier targeting, to reach the brain is dramatically affected by the disease state, Nanomedicine 13 (2018) 585–594.
[4] J. Lalani, M. Rathi, M. Lalan, A. Misra, Protein functionalized tramadol-loaded PLGA nanoparticles: preparation, optimization, stability and pharmacodynamic studies, Drug Dev. Ind. Pharm. 39 (2013) 854–864.
[5] H. Gao, Progress and perspectives on targeting nanoparticles for brain drug delivery, Acta Pharma. Sinica B 6 (2016) 268–286.
[6] S. Krol, Challenges in drug delivery to the brain: nature is against us, J. Contr. Rel. 164 (2012) 145–155.
[7] Z. Liu, X. Gao, T. Kang, M. Jiang, D. Miao, G. Gu, Q. Hu, Q. Song, L. Yao, Y. Tu, B6 peptide-modified PEG-PLA nanoparticles for enhanced brain delivery of neuroprotective peptide, Bioconjugate Chem. 24 (2013) 997–1007.
[8] E. Salvati, F. Re, S. Sesana, I. Cambianica, G. Sancini, M. Masserini, M. Gregori, Liposomes functionalized to overcome the blood–brain barrier and to target amyloid-β peptide: the chemical design affects the permeability across an in vitro model, Int. J. Nanomed. 8 (2013) 1749.
[9] S. Mourtas, A.N. Lazar, E. Markoutsa, C. Duyckaerts, S.G. Antimisiaris, Multifunctional nanoliposomes with curcumin–lipid derivative and brain targeting functionality with potential applications for Alzheimer disease, Eur. J. Med. Chem. 80 (2014) 175–183.
[10] Y. Yu, Z. Pang, W. Lu, Q. Yin, H. Gao, X. Jiang, Self-assembled polymersomes conjugated with lactoferrin as novel drug carrier for brain delivery, Pharm. Res. 29 (2012) 83–96.
[11] K. Hu, J. Li, Y. Shen, W. Lu, X. Gao, Q. Zhang, X. Jiang, Lactoferrin-conjugated PEG–PLA nanoparticles with improved brain delivery: in vitro and in vivo evaluations, J. Contr. Rel. 134 (2009) 55–61.
[12] F. Re, I. Cambianica, C. Zona, S. Sesana, M. Gregori, R. Rigolio, B. La Ferla, F. Nicotra, G. Forloni, A. Cagnotto, Functionalization of liposomes with ApoE-derived peptides at different density affects cellular uptake and drug transport across a blood-brain barrier model, Nanomedicine NBM 7 (2011) 551–559.
[13] L. Bana, S. Minniti, E. Salvati, S. Sesana, V. Zambelli, A. Cagnotto, A. Orlando, E. Cazzaniga, R. Zwart, W. Scheper, Liposomes bi-functionalized with phosphatidic acid and an ApoE-derived peptide affect Aβ aggregation features and cross the blood–brain-barrier: implications for therapy of Alzheimer disease, Nanomedicine NBM 10 (2014) 1583–1590.
[14] A. Cox, P. Andreozzi, R. Dal Magro, F. Fiordaliso, A. Corbelli, L. Talamini, C. Chinello, F. Raimondo, F. Magni, M. Tringali, Evolution of nanoparticle protein corona across the blood-brain barrier, ACS Nano 12 (2018) 7292–7300.
[15] Y. Kanoh, T. Ohara, M. Kanoh, T. Akahoshi, Serum matrix metalloproteinase-2 levels indicate blood–CSF barrier damage in patients with infectious meningitis, Inflammation 31 (2008) 99–104.
[16] B.J. Blyth, A. Farhavar, C. Gee, B. Hawthorn, H. He, A. Nayak, V. Stöcklein, J.J. Bazarian, Validation of serum markers for blood-brain barrier disruption in traumatic brain injury, J. Neurotrauma 26 (2009) 1497–1507.
[17] A. Di Pardo, S. Castaldo, L. Capocci, E. Amico, V. Maglione, Assessment of blood-brain barrier permeability by intravenous infusion of FITC-labeled albumin in a mouse model of neurodegenerative disease, JoVE (J. Visualiz. Exp.) (2017) e56389-e56389.
[18] S. Janelidze, J. Hertze, K. Nägga, K. Nilsson, C. Nilsson, M. Wennström, D. van Westen, K. Blennow, H. Zetterberg, O. Hansson, Increased blood-brain barrier permeability is associated with dementia and diabetes but not amyloid pathology or APOE genotype, Neurobiol. Aging 51 (2017) 104–112.
[19] T. Asano, H. Ito, Y. Kariya, K. Hoshi, A. Yoshihara, Y. Ugawa, H. Sekine, S. Hirohata, Y. Yamaguchi, S. Sato, Evaluation of blood-brain barrier function by quotient alpha2 macroglobulin and its relationship with interleukin-6 and complement component 3 levels in neuropsychiatric systemic lupus erythematosus, PLoS ONE 12 (2017) e0186414.
[20] P.E.H. Jensen, S.H. Jørgensen, P. Datta, P.S. Sørensen, Significantly increased fractions of transformed to total α2-macroglobulin concentrations in plasma from patients with multiple sclerosis, Biochim. et Biophys. Acta (BBA)-Mole. Basis Dis. 1690 (2004) 203–207.
[21] L. Cucullo, N. Marchi, M. Marroni, V. Fazio, S. Namura, D. Janigro, Blood-brain barrier damage induces release of α2-macroglobulin, Mol. Cell. Proteom. 2 (2003) 234–241.
[22] M. Häusler, C. Schäfer, C. Osterwinter, W. Jahnen-Dechent, The physiologic development of fetuin-a serum concentrations in children, Pediatr. Res. 66 (2009) 660.
[23] G.A. Laughlin, L.K. McEvoy, E. Barrett-Connor, L.B. Daniels, J.H. Ix, Fetuin-A, a new vascular biomarker of cognitive decline in older adults, Clin. Endocrinol. 81 (2014) 134–140.
[24] T. Lin, P. Zhao, Y. Jiang, Y. Tang, H. Jin, Z. Pan, H. He, V.C. Yang, Y. Huang, Blood–brain-barrier-penetrating albumin nanoparticles for biomimetic drug delivery via albumin-binding protein pathways for antiglioma therapy, ACS Nano 10 (2016) 9999–10012.
[25] J. Li, L. Feng, L. Fan, Y. Zha, L. Guo, Q. Zhang, J. Chen, Z. Pang, Y. Wang, X. Jiang, Targeting the brain with PEG–PLGA nanoparticles modified with phage-displayed peptides, Biomaterials 32 (2011) 4943–4950.
[26] J. Nicolas, S. Mura, D. Brambilla, N. Mackiewicz, P. Couvreur, Design, functionalization strategies and biomedical applications of targeted biodegradable/biocompatible polymer-based nanocarriers for drug delivery, Chem. Soc. Rev. 42 (2013) 1147–1235.
[27] J. Kreuter, Drug delivery to the central nervous system by polymeric nanoparticles: what do we know? Adv. Drug Deliv. Rev. 71 (2014) 2–14.
[28] J. Kreuter, Influence of the surface properties on nanoparticle-mediated transport of drugs to the brain, J. Nanosci. Nanotechnol. 4 (2004) 484–488.
[29] T.M. Göppert, R.H. Müller, Polysorbate-stabilized solid lipid nanoparticles as colloidal carriers for intravenous targeting of drugs to the brain: comparison of plasma protein adsorption patterns, J. Drug Target. 13 (2005) 179–187.
[30] P. Di Pietro, N. Caporarello, C.D. Anfuso, G. Lupo, A. Magrì, D. La Mendola, C. Satriano, Immobilization of neurotrophin peptides on gold nanoparticles by direct and lipid-mediated interaction: a new multipotential therapeutic nanoplatform for CNS disorders, ACS Omega 2 (2017) 4071–4079.
[31] V. Delplace, P. Couvreur, J. Nicolas, Recent trends in the design of anticancer polymer prodrug nanocarriers, Polym. Chem. 5 (2014) 1529–1544.
[32] D. Vinciguerra, J. Tran, J. Nicolas, Telechelic polymers from reversible-deactivation radical polymerization for biomedical applications, Chem. Commun. 54 (2018) 228–240.
[33] A. Gaudin, M. Yemisci, H. Eroglu, S. Lepetre-Mouelhi, O.F. Turkoglu, B. Dönmez-Demir, S. Caban, M.F. Sargon, S. Garcia-Argote, G. Pieters, Squalenoyl adenosine nanoparticles provide neuroprotection after stroke and spinal cord injury, Nat. Nanotechnol. 9 (2014) 1054.
[34] B.B. Fredholm, A.P. IJzerman, K.A. Jacobson, K.-N. Klotz, J. Linden, International Union of Pharmacology. XXV. Nomenclature and classification of adenosine receptors, Pharmacol. Rev., 53 (2001) pp. 527–552.
[35] C. Londos, D. Cooper, J. Wolff, Subclasses of external adenosine receptors, Proc. Natl. Acad. Sci. 77 (1980) 2551–2554.
[36] G. Haskó, B.N. Cronstein, Adenosine: an endogenous regulator of innate immunity, Trends Immunol. 25 (2004) 33–39.
[37] S. Harrisson, P. Couvreur, J. Nicolas, SG1 nitroxide-mediated polymerization of isoprene: alkoxyamine structure/control relationship and α, ω–chain-end functionalization, Macromolecules 44 (2011) 9230–9238.
[38] D. Vinciguerra, S. Denis, J. Mougin, M. Jacobs, Y. Guillaneuf, S. Mura, P. Couvreur, J. Nicolas, A facile route to heterotelechelic polymer prodrug nanoparticles for imaging, drug delivery and combination therapy, J. Contr. Rel. 286 (2018) 425–438.
[39] M.D. Erion, K.R. Reddy, S.H. Boyer, M.C. Matelich, J. Gomez-Galeno, R.H. Lemus, B.G. Ugarkar, T.J. Colby, J. Schanzer, P.D. van Poelje, Design, synthesis, and characterization of a series of cytochrome P450 3A-activated prodrugs (hepdirect prodrugs) useful for targeting phosph (on) ate-based drugs to the liver §, J. Am. Chem. Soc. 126 (2004) 5154–5163.
[40] D. Benoit, V. Chaplinski, R. Braslau, C.J. Hawker, Development of a universal alkoxyamine for "living" free radical polymerizations, J. Am. Chem. Soc. 121 (1999) 3904–3920.
[41] D. Benoit, E. Harth, P. Fox, R.M. Waymouth, C.J. Hawker, Accurate structural control and block formation in the living polymerization of 1, 3-dienes by nitroxide-mediated procedures, Macromolecules 33 (2000) 363–370.
[42] S. Harrisson, J. Nicolas, A. Maksimenko, D.T. Bui, J. Mougin, P. Couvreur, Nanoparticles with in vivo anticancer activity from polymer prodrug amphiphiles prepared by living radical polymerization, Angew. Chem. Int. Ed. 52 (2013) 1678–1682.
[43] N. Sankaran, A.Z. Rys, R. Nassif, M.K. Nayak, K. Metera, B. Chen, H.S. Bazzi, H.F. Sleiman, Ring-opening metathesis polymers for biodetection and signal amplification: synthesis and self-assembly, Macromolecules 43 (2010) 5530–5537.
[44] K. Matsumoto, T. Iwata, M. Suenaga, Mild oxidation of alcohols using soluble polymer-supported TEMPO in combination with oxone: effect of a basic matrix of TEMPO derivatives, Heterocycles 81 (2010) 2539–2553.
[45] H. Fessi, F. Puisieux, J.P. Devissaguet, N. Ammoury, S. Benita, Nanocapsule formation by interfacial polymer deposition following solvent displacement, Int. J. Pharm. 55 (1989) R1–R4.
[46] G. Sancini, M. Gregori, E. Salvati, I. Cambianica, F. Re, F. Ornaghi, M. Canovi, C. Fracasso, A. Cagnotto, M. Colombo, C. Zona, M. Gobbi, M. Salmona, B. La Ferla, F. Nicotra, M. Masserini, Functionalization with TAT-peptide enhances blood-brain barrier crossing in vitro of nanoliposomes carrying a curcumin-derivative to bind amyloid-b peptide, J. Nanomed. Nanotechol. 4 (2013) 171–178.
[47] P. Grossen, G. Québatte, D. Witzigmann, C. Prescianotto-Baschong, L.-H. Dieu, J. Huwyler, Functionalized solid-sphere PEG-b-PCL nanoparticles to target brain

capillary endothelial cells in vitro, J. Nanomater. 2016 (2016) 13.
[48] A. Cox, P. Andreozzi, R. Dal Magro, F. Fiordaliso, A. Corbelli, L. Talamini, C. Chinello, F. Raimondo, F. Magni, M. Tringali, Evolution of nanoparticle protein corona across the blood-brain barrier, ACS Nano (2018).
[49] A. Gaudin, O. Tagit, D. Sobot, S. Lepetre-Mouelhi, J. Mougin, T.F. Martens, K. Braeckmans, V.R. Nicolas, D. Desmaële, S.C. de Smedt, Transport mechanisms of squalenoyl-adenosine nanoparticles across the blood–brain barrier, Chem. Mater. 27 (2015) 3636–3647.
[50] B. Weksler, I.A. Romero, P.-O. Couraud, The hCMEC/D3 cell line as a model of the human blood brain barrier, Fluids Barrier. CNS 10 (2013) 16.
[51] R. Cecchelli, B. Dehouck, L. Descamps, L. Fenart, V. Buée-Scherrer, C. Duhem, S. Lundquist, M. Rentfel, G. Torpier, M.-P. Dehouck, In vitro model for evaluating drug transport across the blood–brain barrier, Adv. Drug Deliv. Rev. 36 (1999) 165–178.
[52] M. Gregori, A. Orlando, F. Re, S. Sesana, L. Nardo, D. Salerno, F. Mantegazza, E. Salvati, A. Zito, F. Malavasi, Novel antitransferrin receptor antibodies improve the blood–brain barrier crossing efficacy of immunoliposomes, J. Pharm. Sci. 105 (2016) 276–283.
[53] W. Ma, A. Saccardo, D. Roccatano, D. Aboagye-Mensah, M. Alkaseem, M. Jewkes, F. Di Nezza, M. Baron, M. Soloviev, E. Ferrari, Modular assembly of proteins on nanoparticles, Nat. Commun. 9 (2018) 1489.
[54] M. Moser, R. Schneider, T. Behnke, T. Schneider, J. Falkenhagen, U. Resch-Genger, Ellman's and aldrithiol assay as versatile and complementary tools for the quantification of thiol groups and ligands on nanomaterials, Anal. Chem. 88 (2016) 8624–8631.
[55] J. Nicolas, Drug-initiated synthesis of polymer prodrugs: combining simplicity and efficacy in drug delivery, Chem. Mater. 28 (2016) 1591–1606.
[56] E. Guégain, J. Tran, Q. Deguettes, J. Nicolas, Degradable polymer prodrugs with adjustable activity from drug-initiated radical ring-opening copolymerization, Chem. Sci. (2018).
[57] Y. Bao, T. Boissenot, E. Guégain, D. Desmaële, S. Mura, P. Couvreur, J. Nicolas, Simple synthesis of cladribine-based anticancer polymer prodrug nanoparticles with tunable drug delivery properties, Chem. Mater. 28 (2016) 6266–6275.
[58] Y. Bao, E. Guégain, V. Nicolas, J. Nicolas, Fluorescent polymer prodrug nanoparticles with aggregation-induced emission (AIE) properties from nitroxide-mediated polymerization, Chem. Commun. 53 (2017) 4489–4492.
[59] Y. Bao, E. Guégain, J. Mougin, J. Nicolas, Self-stabilized, hydrophobic or PEGylated paclitaxel polymer prodrug nanoparticles for cancer therapy, Polym. Chem. 9 (2018) 687–698.
[60] D. Trung Bui, A. Maksimenko, D. Desmaële, S. Harrisson, C. Vauthier, P. Couvreur, J. Nicolas, Polymer prodrug nanoparticles based on naturally occurring isoprenoid for anticancer therapy, Biomacromolecules 14 (2013) 2837–2847.
[61] A. Maksimenko, D.T. Bui, D. Desmaële, P. Couvreur, J. Nicolas, Significant tumor growth inhibition from naturally occurring lipid-containing polymer prodrug nanoparticles obtained by the drug-initiated method, Chem. Mater. 26 (2014) 3606–3609.
[62] Y. Bao, J. Nicolas, Structure–cytotoxicity relationship of drug-initiated polymer prodrug nanoparticles, Polym. Chem. 8 (2017) 5174–5184.
[63] B. Louage, L. Nuhn, M.D. Risseeuw, N. Vanparijs, R. De Coen, I. Karalic, S. Van Calenbergh, B.G. De Geest, Well-defined polymer-paclitaxel prodrugs by a grafting-from-drug approach, Angew. Chem. Int. Ed. 55 (2016) 11791–11796.
[64] B. Louage, M.J. Van Steenbergen, L. Nuhn, M.D. Risseeuw, I. Karalic, J. Winne, S. Van Calenbergh, W.E. Hennink, B.G. De Geest, Micellar paclitaxel-initiated RAFT polymer conjugates with acid-sensitive behavior, ACS Macro Lett. 6 (2017) 272–276.
[65] H.-C. Yang, J. Silverman, J.J. Wozniak, Low temperature heat shrinkable polymer material, in, Google Patents, 1986.
[66] D. Vinciguerra, M. Jacobs, S. Denis, J. Mougin, Y. Guillaneuf, G. Lazzari, C. Zhu, S. Mura, P. Couvreur, J. Nicolas, Heterotelechelic polymer prodrug nanoparticles: adaptability to different drug combinations and influence of the dual functionalization on the cytotoxicity, J. Contr. Rel. 295 (2019) 223–236.
[67] K.L. Heredia, H.D. Maynard, Synthesis of protein–polymer conjugates, Org. Biomol. Chem. 5 (2006) 45–53.
[68] J. Nicolas, G. Mantovani, D.M. Haddleton, Living radical polymerization as a tool for the synthesis of polymer-protein/peptide bioconjugates, Macromol. Rapid Commun. 28 (2007) 1083–1111.
[69] M.A. Gauthier, H.-A. Klok, Peptide/protein–polymer conjugates: synthetic strategies and design concepts, Chem. Commun. 2591–2611 (2008).
[70] R. Benson, R. Meyer, M. Zaruba, G. McKhann, Cellular autofluorescence–is it due to flavins? J. Histochem. Cytochem. 27 (1979) 44–48.
[71] T. Nguyen, M.B. Francis, Practical synthetic route to functionalized rhodamine dyes, Org. Lett. 5 (2003) 3245–3248.
[72] A. Gessner, R. Waicz, A. Lieske, B.-R. Paulke, K. Mäder, R. Müller, Nanoparticles with decreasing surface hydrophobicities: influence on plasma protein adsorption, Int. J. Pharm. 196 (2000) 245–249.
[73] C.D. Walkey, J.B. Olsen, H. Guo, A. Emili, W.C. Chan, Nanoparticle size and surface chemistry determine serum protein adsorption and macrophage uptake, J. Am. Chem. Soc. 134 (2012) 2139–2147.
[74] S. Nandhakumar, M.D. Dhanaraju, V.D. Sundar, B. Heera, Influence of surface charge on the in vitro protein adsorption and cell cytotoxicity of paclitaxel loaded poly(ε-caprolactone) nanoparticles, Bull. Fac. Pharm., Cairo Univ. 55 (2017) 249–258.
[75] Z.J. Deng, M. Liang, I. Toth, M. Monteiro, R.F. Minchin, Plasma protein binding of positively and negatively charged polymer-coated gold nanoparticles elicits different biological responses, Nanotoxicology 7 (2012) 314–322.
[76] T. Yang, D. Sun, P. Xu, S. Li, Y. Cen, Y. Li, Q. Xu, Y. Sun, W. Li, Y. Lin, Stability of bovine serum albumin labelled by rhodamine B isothiocyanate, Biomed. Res. 28 (2017).
[77] G. Sinigaglia, M. Magro, G. Miotto, S. Cardillo, E. Agostinelli, R. Zboril, E. Bidollari, F. Vianello, Catalytically active bovine serum amine oxidase bound to fluorescent and magnetically drivable nanoparticles, Int. J. Nanomed. 7 (2012) 2249–2259.
[78] S. Patil, A. Sandberg, E. Heckert, W. Self, S. Seal, Protein adsorption and cellular uptake of cerium oxide nanoparticles as a function of zeta potential, Biomaterials 28 (2007) 4600–4607.
[79] M. Li, S. Mosel, S.K. Knauer, C. Schmuck, A dipeptide with enhanced anion binding affinity enables cell uptake and protein delivery, Org. Biomol. Chem. 16 (2018) 2312–2317.
[80] B. Weksler, E. Subileau, N. Perriere, P. Charneau, K. Holloway, M. Leveque, H. Tricoire-Leignel, A. Nicotra, S. Bourdoulous, P. Turowski, Blood-brain barrier-specific properties of a human adult brain endothelial cell line, FASEB J. 19 (2005) 1872–1874.
[81] I. Rombouts, B. Lagrain, K.A. Scherf, M.A. Lambrecht, P. Koehler, J.A. Delcour, Formation and reshuffling of disulfide bonds in bovine serum albumin demonstrated using tandem mass spectrometry with collision-induced and electron-transfer dissociation, Sci. Rep. 5 (2015) 12210.
[82] M.-A. Ghetie, J.W. Uhr, E.S. Vitetta, Covalent binding of human α2-macroglobulin to deglycosylated ricin A chain and its immunotoxins, Cancer Res. 51 (1991) 1482–1487.
[83] K. Dziegielewska, W. Brown, S. Casey, D. Christie, R. Foreman, R. Hill, N. Saunders, The complete cDNA and amino acid sequence of bovine fetuin. Its homology with alpha 2HS glycoprotein and relation to other members of the cystatin superfamily, J. Biol. Chem. 265 (1990) 4354–4357.
[84] N. Sathyamoorthy, D.D. Magharla, S.D. Vankayalu, Effect of surface modification on the In vitro protein adsorption and cell cytotoxicity of vinorelbine nanoparticles, J. Pharm. Bioallied Sci. 9 (2017) 135.
[85] E.P. Ivanova, J.P. Wright, D.K. Pham, N. Brack, P. Pigram, Y.V. Alekseeva, G.M. Demyashev, D.V. Nicolau, A comparative study between the adsorption and covalent binding of human immunoglobulin and lysozyme on surface-modified poly (tert-butyl methacrylate), Biomed. Mater. 1 (2006) 24.
[86] N.V. Konduru, R.M. Molina, A. Swami, F. Damiani, G. Pyrgiotakis, P. Lin, P. Andreozzi, T.C. Donaghey, P. Demokritou, S. Krol, Protein corona: implications for nanoparticle interactions with pulmonary cells, Part. Fibre Toxicol. 14 (2017) 42.
[87] N.V. Konduru, R.M. Molina, A. Swami, F. Damiani, G. Pyrgiotakis, P. Lin, P. Andreozzi, T.C. Donaghey, P. Demokritou, S. Krol, W. Kreyling, J.D. Brain, Protein corona: implications for nanoparticle interactions with pulmonary cells, Part. Fibre Toxicol. 14 (2017) 42.
[88] B.-J.L. Van Hong Nguyen, Protein corona: a new approach for nanomedicine design, Int. J. Nanomed. 12 (2017) 3137.
[89] D. Dutta, S.K. Sundaram, J.G. Teeguarden, B.J. Riley, L.S. Fifield, J.M. Jacobs, S.R. Addleman, G.A. Kaysen, B.M. Moudgil, T.J. Weber, Adsorbed proteins influence the biological activity and molecular targeting of nanomaterials, Toxicol. Sci. 100 (2007) 303–315.
[90] I. Schütz, T. Lopez-Hernandez, Q. Gao, D. Puchkov, S. Jabs, D. Nordmeyer, M. Schmudde, E. Rühl, C.M. Graf, V. Haucke, Lysosomal dysfunction caused by cellular accumulation of silica nanoparticles, J. Biol. Chem. (2016) jbc. M115. 710947.
[91] S. Barua, S. Mitragotri, Synergistic targeting of cell membrane, cytoplasm, and nucleus of cancer cells using rod-shaped nanoparticles, ACS Nano 7 (2013) 9558–9570.
[92] M.P. Monopoli, C. Åberg, A. Salvati, K.A. Dawson, Biomolecular coronas provide the biological identity of nanosized materials, Nat. Nanotechnol. 7 (2012) 779.
[93] S. Petrash, T. Cregger, B. Zhao, E. Pokidysheva, M.D. Foster, W.J. Brittain, V. Sevastianov, C.F. Majkrzak, Changes in protein adsorption on self-assembled monolayers with monolayer order: comparison of human serum albumin and human gamma globulin, Langmuir 17 (2001) 7645–7651.
[94] R.A. Vijayendran, D.E. Leckband, A quantitative assessment of heterogeneity for surface-immobilized proteins, Anal. Chem. 73 (2001) 471–480.